Adaptive Control Of Woofer-Tweeter Adaptive Optics

THESIS

Jimmie J. Perez, Captain, USAF

AFIT/GE/ENG/09-33

DEPARTMENT OF THE AIR FORCE
AIR UNIVERSITY

AIR FORCE INSTITUTE OF TECHNOLOGY

Wright-Patterson Air Force Base, Ohio

The views expressed in this thesis are those of the author and do not reflect the official policy or position of the United States Air Force, Department of Defense, or the United States Government.

AFIT/GE/ENG/09-33

Adaptive Control Of Woofer-Tweeter Adaptive Optics

THESIS

Presented to the Faculty

Department of Electrical and Computer Engineering

Graduate School of Engineering and Management

Air Force Institute of Technology

Air University

Air Education and Training Command

In Partial Fulfillment of the Requirements for the

Degree of Master of Science in Electrical Engineering

Jimmie J. Perez, B.S.E.E.

Captain, USAF

March 2009

AFIT/GE/ENG/09-33

Adaptive Control Of Woofer-Tweeter Adaptive Optics

Jimmie J. Perez, B.S.E.E.
Captain, USAF

Approved:

Gregory J. Toussaint	24 Feb 2009
Lt Col Gregory J. Toussaint, PhD (Chairman)	date
Jason D. Schmidt	24 Feb 09
Maj Jason D. Schmidt, PhD (Member)	date
Salvatore J. Cusumano	24 Feb 2009
Dr. Salvatore J. Cusumano (Member)	date

AFIT/GE/ENG/09-33

Abstract

Adaptive optics applies advanced sensing and control to improve the ability of optical systems to collect images through a turbulent atmosphere. The results of this research effort demonstrate that the combination of two recent approaches improves the performance of adaptive optics in directed energy and laser communication scenarios. The first approach is adaptive control, which offers improved performance over fixed-gain controllers in the presence of rapidly changing turbulence. The second approach incorporated into the study is a dual-mirror system. The two mirrors are a high-bandwidth, low-actuator-stroke (tweeter) mirror and a low-bandwidth, large-actuator-stroke (woofer) mirror. The woofer-tweeter combination allows for better compensation of the large-variance, high-spatial-frequency phase distortion generated by strong turbulence. Two different adaptive controllers are presented, one using a relatively simple model reference adaptive system controller and one using a lattice filter controller. The lattice filter is implemented in two ways. In one implementation the filter operates on the individual actuators, while in the other it operates on frequency weighted modes. The modal implementation reduces the computational burden of the filter. The performance of the different adaptive controllers is compared to both each other and to a traditional fixed-gain controller. Simulations show that adaptive control of woofer-tweeter AO can increase the mean Strehl ratio by up to 20%. In general, the lattice filter controllers outperform the model reference adaptive system controller. However, in cases where the lattice filter cannot use a sufficient number of modes, the model reference adaptive system can outperform the lattice filter.

Acknowledgements

I owe a large debt of gratitude to all those who offered me their support while working on my thesis. First, and foremost, I would like to thank my wife for her understanding and patience as I worked many long nights and weekends. She also graciously agreed to proof read all the various drafts of my thesis and ended up reviewing hundreds of pages, even though she doesn't understand all the content. I would also like to thank my advisor, Lt Col Gregory Toussaint, for his constant feedback on my research and invaluable advice. When I had problems with my research, his suggestions always helped guide me to a solution. My committee members, Maj Jason Schmidt and Dr. Salvatore Cusumano, were extremely helpful and patient with my optics questions. I owe a special thanks to Maj Schmidt for helping me identify and work through some of the quirks in the simulation software. I would also like to thank my parents for always making education a priority and driving me to always do my best. Last, I would like to thank my friends and colleagues Maj Dulksi, Capt Groves, and Capt Engstrom for their help with optics questions, their honest feedback on my work, and for helping me keep my sanity through all the long hours.

Jimmie J. Perez

Table of Contents

Page

List of Figures

List of Tables

List of Symbols

Symbol		Page
B_n	Refractive index covariance	4
$\langle \cdot \rangle$	Expectation operator	4
$\Phi(K)$	Atmospheric power spectral density	4
l_0	Inner scale	5
L_0	Outer scale	5
K	Three-dimensional spatial-frequency	5
C_n^2	Atmospheric structure constant	6
r_0	Fried's parameter	6
k	Wave number	6
λ	Wavelength	6
z	Altitude	7
β	Zenith angle	7
θ_0	Isoplanatic angle	7
f_G	Greenwood frequency	7
τ_0	Greenwood time constant	7
$V(z)$	Wind velocity	7
y	Measurement vector	12
c	Actuator commands	12
Γ	Poke matrix	12
$\varphi(\mathbf{r})$	Atmospheric phase	18
M	Number of lattice filter stages	23
κ_m	Reflection coefficient	23
$f_m(n)$	Forward prediction error	24
$b_m(n)$	Backward prediction error	24
Δt	Simulation time step	29

List of Abbreviations

Abbreviation		Page
AO	Adaptive Optics	1
BIBO	Bounded-Input Bounded-Output	23
DM	Deformable Mirror	4
FIR	Finite Impulse Response	22
GAL	Gradient Adaptive Lattice	37
MRAS	Model Reference Adaptive System	21
OPD	Optical Path Difference	9
SH WFS	Shack-Hartmann Wavefront Sensor	10
SISO	Single-Input Single-Output	16
SRI WFS	Self-Referencing Interferometer Wavefront Sensor	14
WCE	Wavefront Control Experiment	12
WFS	Wavefront Sensor	4

Adaptive Control Of Woofer-Tweeter Adaptive Optics

I. Introduction

Adaptive optics (AO) refers to a closed-loop optical system whose purpose is to correct for atmospheric aberrations. In astronomical applications, adaptive optics is used to reduce the distortion of the incoming light and improve the image. In laser communication and directed-energy applications, an AO system pre-distorts the outgoing light. Then, the atmosphere corrects the pre-distortion which results in a more focused spot at the target and, consequently, more energy on the target.

There are two recent approaches to improve the performance of adaptive optics in directed energy and laser communication scenarios. The first approach is adaptive control, which offers improved performance over fixed-gain controllers in the presence of rapidly changing turbulence. The second approach is a dual-mirror system. The two mirrors are a high-bandwidth, low-actuator-stroke (tweeter) mirror and a low-bandwidth, large-actuator-stroke (woofer) mirror. The woofer-tweeter combination allows for better compensation of the large-variance, high-spatial-frequency phase distortion generated by strong turbulence. This research combines these two approaches.

1.1 Problem Statement

The objective of this research is to develop an adaptive controller for a woofer-tweeter AO system which improves the performance of the system compared to traditional fixed-gain controllers. The controller design is verified using wave-optics simulations in different atmospheric turbulence scenarios.

The particular goals of this research are:

- to determine a control architecture suitable for implementing an adaptive controller with a woofer-tweeter AO system,
- to develop an adaptive controller using the determined control architecture, which improves the performance of a woofer-tweeter AO system,
- to reduce the computational complexity of the controller through the use of modal decomposition,
- to use wave-optics simulations to demonstrate the improvement gained by using an adaptive controller,
- and to compare the improvement with various implementations of the adaptive controller.

This research effort realized all of the stated goals. The analysis shows that an adaptive controller improves the performance of woofer-tweeter AO systems and adaptive control of woofer-tweeter AO is a viable approach to compensating strong, fast-moving turbulence.

1.2 Thesis Overview

Chapter II discusses the topic of atmospheric turbulence and its mathematical description. It then provides a brief overview of AO systems and their major components, including commonly used controllers. After covering typical AO systems, woofer-tweeter AO systems are discussed. First, the need for woofer-tweeter AO is established followed by a discussion on woofer-tweeter controllers. The last section in Chapter II defines adaptive control, covers two types of adaptive control techniques, and discusses current applications of adaptive control and AO, including modal decomposition.

Chapter III gives details on the parameters used to model the atmospheric turbulence and the AO system hardware. These parameters are needed to derive the specific control laws used in the adaptive controllers, as well as define the simulations. With the required system parameters established, three different controllers are derived using the techniques discussed in Chapter II.

Chapter IV implements the controllers designed in Chapter III. First, a baseline for comparing the different controllers is established using a standard woofer-tweeter system. Each controller is then simulated. The simulations are used to determine the best implementation for each controller. Once the specific implementation has been established, the controllers are compared to the baseline system and to each other.

Chapter V summarizes the simulation results and provides a detailed comparison between the different controllers. Based on the evidence presented, a final conclusion is given that adaptive control indeed improves woofer-tweeter AO. Various areas for future work are then recommended. These recommendations propose ways to use or build upon the adaptive control algorithms presented.

II. Background and Current Research

This chapter gives a brief overview of conventional adaptive optics systems, including the major components and common control designs. Two areas of recent interest to the AO community, woofer-tweeter AO and adaptive control, are also discussed. The topics presented in this chapter form the foundation of the adaptive woofer-tweeter controller design presented in Chapter III.

2.1 Conventional AO

A typical AO system uses the following components: a wavefront sensor (WFS) to measure the light from a source beacon, a deformable mirror (DM) to adjust the waves, and a control computer to translate the WFS measurements into DM commands. To better understand AO, the following four sections discuss atmospheric turbulence, deformable mirrors, wavefront sensors, and control. Figure 2.1 shows how these components are used in a typical AO system.

2.1.1 Atmospheric Turbulence. In order to understand AO systems, it is necessary to understand how the atmosphere affects light and how to describe and quantify these effects. Because air has an index of refraction that is not exactly one, light is bent as it travels through the air. The index of refraction depends on the pressure, density, and temperature of the air as well as the frequency of the light. In a given mass of air, the pressure, density, and temperature vary throughout the mass. These variations result in pockets of differing indices of refraction. The covariance of the refractive index, B_n, can be computed by comparing the refractive index at one point, $n_1(r_1)$, with another point, $n_1(r + r_1)$, and averaging over the air mass of interest according to

$$B_n(r) = \langle n_1(r + r_1)\ n_1(r_1) \rangle \tag{2.1}$$

where r_1 is the position in the air mass, r is the distance between the points, and $\langle \cdot \rangle$ is the expectation operator. The power spectral density, $\Phi(K)$, of the atmosphere is

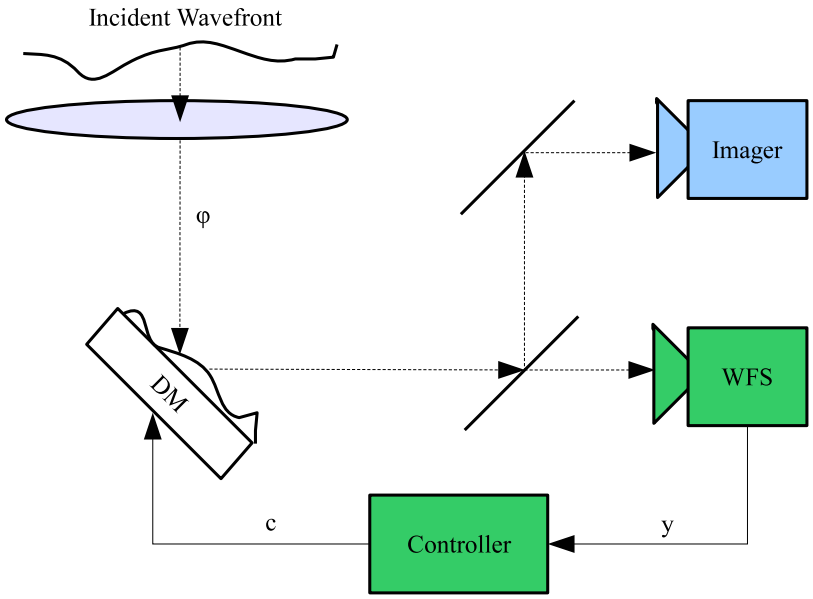

Figure 2.1: A typical AO system including: a wavefront sensor (WFS), deformable mirror (DM), and a control computer [21].

the three-dimensional Fourier transform of the covariance give by

$$\Phi(K) = \frac{1}{(2\pi)^3} \int_{l_o}^{L_0} B_n(r) \exp(-K \cdot r) d^3 r \tag{2.2}$$

where l_0 is the inner scale, or smallest atmospheric eddy size, L_0 is the outer scale, or largest atmospheric eddy size, and K is the three-dimensional spatial-frequency [20]. In general, this integral does not have a closed-form solution. However, with certain assumptions a closed-form solution can be found. Two of the most common solutions are the Kolmogorov spectrum and the Von Kármán spectrum. In the Kolmogorov spectrum, the inner scale is zero and the outer scale is finite, which yields the following expression for the power spectral density:

$$\Phi(K) = 0.033 C_n^2 K^{-11/3} \tag{2.3}$$

In the Von Kármán spectrum, the inner scale is zero and the outer scale is finite and yields the following:

$$\Phi(K) = 3.9 \times 10^{-5} C_n^2 L_0^{11/3} \left[1 + \frac{L_0^2 K^2}{(2\pi)^2}\right]^{-11/6} \tag{2.4}$$

In both equations the atmospheric structure constant, C_n^2, represents the severity of the turbulence and typically ranges between 10^{-15} $\mathrm{m}^{-2/3}$ and 10^{-18} $\mathrm{m}^{-2/3}$ as a function of altitude [20]. For simulation purposes, several canonical models of C_n^2 exist within the AO community [20].

The various pockets of air with different refractive indices can be thought of as a collection of lenses floating in the air. Coherent light passing through these eddies becomes spatially decorrelated at an aperture because light arriving at different points of the aperture travels through different paths. A common metric describing the strength of the turbulence is Fried's parameter, r_0. This parameter refers to the largest aperture over which light would be coherent for a given turbulence. In other words, a benign atmosphere with no turbulence would have $r_0 = \infty$. As the atmosphere becomes more turbulent, the value of r_0 decreases. Thus, smaller values of r_0 indicate a more severe turbulence. If Kolmogorov turbulence is assumed, the coherence length for a plane wave is

$$r_0 = 1.68 \left(C_n^2 L k^2\right)^{-3/5} \tag{2.5}$$

where L is the length of the propagation path and k is the wave number. The wave number is related to the wavelength, λ, by

$$k = \frac{2\pi}{\lambda} \tag{2.6}$$

In astronomical applications and other scenarios with vertical propagation, the structure constant, C_n^2, varies with altitude, z, and zenith angle, β. In this case,

$$r_0 = \left(0.423k^2 \sec\beta \int\limits_{\text{Path}} C_n^2(z)dz \right)^{-3/5} \tag{2.7}$$

for a plane-wave source. Typical values of r_0 range from 5-10 cm.

Another metric to describe atmospheric turbulence is the isoplanatic angle, θ_0. The isoplanatic angle is the angular radius around the beacon that exhibits the same turbulence as the beacon. In other words, an object within θ_0 of the beacon will be properly imaged by the AO system. At a given zenith angle, θ_0 is

$$\theta_0 = \left(2.91k^2 \sec^{8/3}\beta \int\limits_{\text{Path}} C_n^2(z)z^{5/3}dz \right)^{-3/5} \tag{2.8}$$

Typical values of θ_0 are between 7-10 μrad.

All of the metrics presented above describe spatial characteristics of turbulence. One measure of the temporal characteristics of turbulence is the Greenwood frequency, f_G. The inverse of the Greenwood frequency is Greenwood time constant, τ_0. This time constant describes the interval over which turbulence is nearly constant and is given by

$$\tau_0 = \left(2.91k^2 \sec\beta \int\limits_{\text{Path}} C_n^2(z)V^{5/3}(z)dz \right)^{-3/5} \tag{2.9}$$

where $V(z)$ is the wind velocity along the path. If the wind velocity is constant then

$$\tau_0 = 2.34\frac{r_0}{V} \tag{2.10}$$

or equivalently

$$f_G = 0.427\frac{V}{r_0} \tag{2.11}$$

Typical time constants are on the order of milliseconds [2].

The performance of an AO system can be measured by how well it compensates for the atmospheric turbulence. A perfectly compensated wavefront would be a plane wave with uniform phase across the aperture. If this perfect plane wave were imaged it would result in a spot whose intensity is determined by the optical properties of the imaging system. This is known as the diffraction-limited case. An aberrated wavefront results in a less focused spot with reduced intensity. The ratio of the peak aberrated spot intensity to the peak diffraction-limited intensity is known as the Strehl ratio. The Strehl ratio is always between zero and one and is used to measure an AO system's performance. An AO system which perfectly compensates the atmospheric distortion would have Strehl ratio of one. As the wavefront becomes more distorted, the Strehl ratio approaches zero.

Using the atmospheric turbulence models and the metrics described in this section, it is possible to build computer simulations with the appropriate characteristics and measure the performance of a simulated AO system. The simulation scenarios presented in Section 3.1.2 are described in terms of the Fried parameter and the Greenwood frequency. The characteristics of the atmosphere are also essential to understanding the need for two DMs as discussed in Section 2.2. In order to understand how an AO system compensates for turbulence, the following sections describe the components of an AO system.

2.1.2 Deformable Mirrors. The deformable mirror in an AO system allows the system to alter the phase of the light in response to the WFS measurements. The goal of the AO system is to adjust the figure of the DM so it has the same shape as the aberrated wave with the opposite sign. If the aberrated wave is of the form $A\exp(i\phi)$, then the DM ideally imparts the complex conjugate, $A\exp(-i\phi)$, to cancel the aberration.

A deformable mirror consists of a reflective faceplate with actuators below the mirror surface to move it up or down. The actuators change the path length transversed by the light, which changes the phase. Because the light reflects off the mirror,

the change in the total distance traveled by the light is twice the displacement of the actuator, once before reflection and once after reflection. This change in the distance the light travels is known as the optical path difference (OPD). Most DMs fall into one of two categories: segmented and continuous faceplate. For a DM with a segmented faceplate, the surface is not continuous and consists of many small mirrors placed close together. Each small mirror sits atop an actuator which moves it up and down. Due to the segmented design, each actuator influences only the position of the corresponding segment.

In a continuous faceplate DM, the mirror surface is a continuous sheet with an array of actuators below it. As a result, when an actuator moves, its influence is not limited to the mirror region directly above it. The spatial deformation of the mirror surface due to an actuator movement is known as the influence function. The amount of deformation that extends to an adjacent actuator position is called coupling. Figure 2.2 illustrates the differences between the two mirror types.

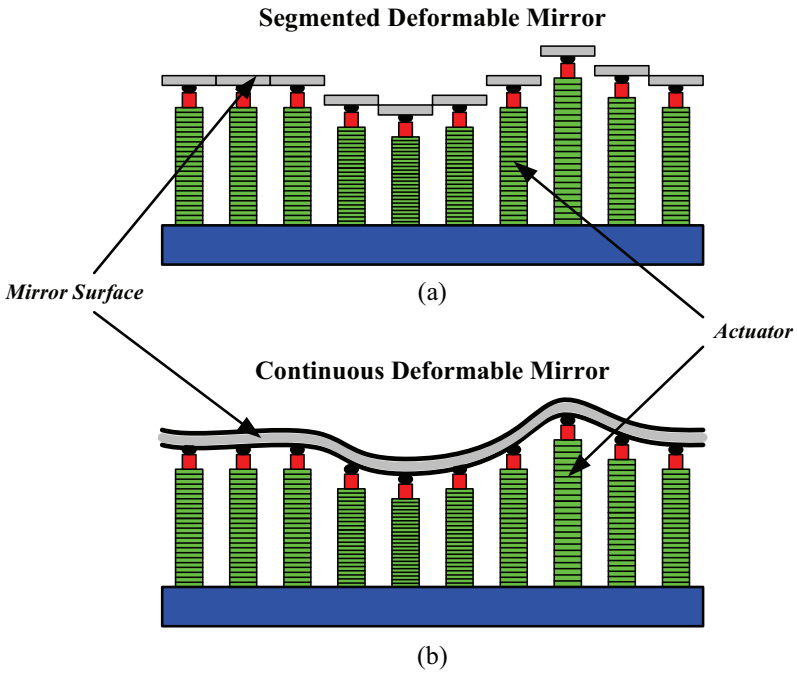

Figure 2.2: There are two types of DMs: (a) segmented and (b) continuous faceplate [21].

Due to their lack of coupling, segmented mirrors are able to correct for aberrations with high spatial-frequency content, provided the individual actuators are sufficiently close. They do, however, suffer from signal loss as light passes through the gaps in the segments and from diffraction effects at their edges. A continuous faceplate DM provides a smooth fit to the wavefront as a result of coupling, which is advantageous when correcting lower-order aberrations.

2.1.3 Wavefront Sensors. In order to control the DM and correct aberrations in phase of the wavefront, it is necessary to measure the light. A wavefront sensor (WFS) provides this measurement. Ideally, a sensor which directly measures the phase of the wavefront would be used. Unfortunately, direct measurements of the phase are not possible. Several methods exist which allow the phase to be inferred from other measurements. The most common WFS, a Shack-Hartmann WFS, uses a non-interferometric approach and measures the spatial derivative, or tilt, of the phase. There are numerous methods which use various implementations of interferometry to create diffraction patterns. The intensity of the diffraction pattern is proportional to the phase of the wavefront. One of the more recent implementations is known as the self-referencing interferometer. This subsection will describe the important elements of these two types of wavefront sensors.

2.1.3.1 Shack-Hartmann WFS. A Shack-Hartmann WFS (SH WFS) is based on a classical optical test known as the Hartmann test. In a Hartmann test, the wavefront of a beam is measured using an array of pinholes to determine the slope of the wavefront over a number of points. If the wave were perfectly planar each pinhole would produce a spot directly behind it. However, if there are aberrations in the wave, they cause the spot position to be shifted by an amount proportional to the wavefront slope at the pinhole location. Instead of an array of pinholes, a SH WFS uses an array of small lenses, called lenslets, to focus the wavefront into spots. By using a lenslet array which captures more light, the SH WFS does not suffer the same signal loss as a pinhole array which only utilizes the small fraction of

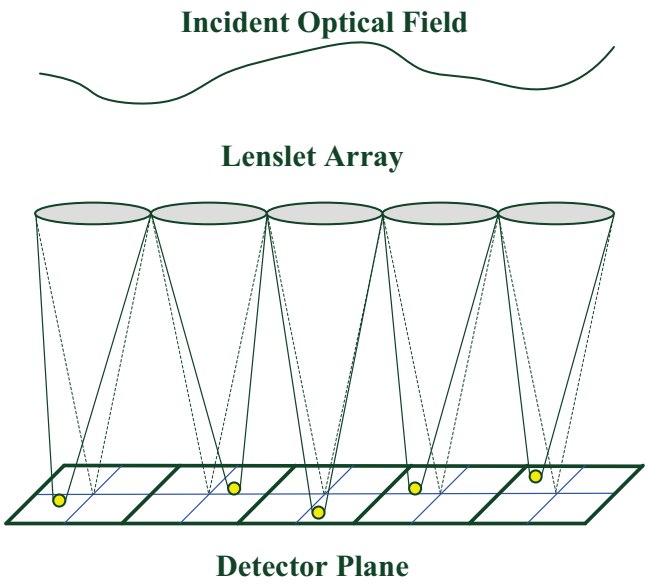

Figure 2.3: Example of a SH WFS using a one-dimensional lenslet array. The lenslet array produces a spot on the detector array. The spatial shift in the spot is proportional to the slope of the wavefront [21].

light which passes through the pinholes. Figure 2.3 shows a one-dimensional example of a SH WFS where each lenslet in a lenslet array focuses a portion of the wavefront to produce a spot on the detector plane. Each spot is displaced from the center of the corresponding section of the detector plane due to the local slope of the wavefront.

One method for determining the shift in the spot location is by using a quadcell detector. A quadcell consists of four closely spaced detectors, as shown in Figure 2.4. The spot's horizontal displacement is calculated by averaging spot intensity of the two left detectors and subtracting the average intensity of the right two detectors. Similarly, the vertical displacement is the difference between the averages of the top and bottom pairs of detectors.

Because the SH WFS does not provide a direct measurement of phase, it is necessary to reconstruct the phase from the WFS measurements in order to drive the DM. To perform the reconstruction, it is essential to know how the WFS and DM are aligned. The alignment geometry refers to the manner in which the WFS measurements relate to the DM actuators. Figure 2.5 shows four of the most common

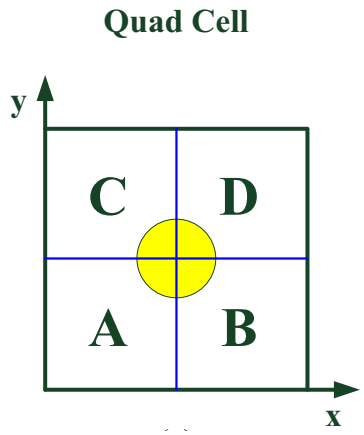

Figure 2.4: A quadcell detector is used in a SH WFS to measure the vertical and horizontal shift of the focused spot. The horizontal displacement is the difference between the left and right average intensities. The vertical displacement is the difference between the top and bottom average intensities [21].

geometries. The Fried geometry measures orthogonal slopes centered between four actuators. The Wavefront Control Experiment (WCE) geometry is identical to the Fried geometry, but is rotated 45°. The Hudgin geometry measures orthogonal slopes between adjacent actuators. The Southwell geometry measures orthogonal slopes at each actuator position.

Once the geometry has been established, the relationship between measurement vector, y, and the actuator commands, c, can be defined. Assuming a linear relationship between the measured wavefront slopes and actuator commands, the relationship is simply

$$\mathbf{y}_{(M\times 1)} = \Gamma_{(M\times N)}\mathbf{c}_{(N\times 1)} \tag{2.12}$$

where the matrix Γ, the poke matrix, represents the system's geometry, actuator coupling, and influence functions and describes how the actuator commands correspond to the WFS measurements. The subscripts denote the dimensions of the variables. In general, $M > N$ and the system is overdetermined. When the system is overdetermined a common method of solving Equation (2.12) is to use the least-squares, or pseudo-inverse solution,

$$c = (\Gamma^T\Gamma)^{-1}\Gamma^T\Gamma y \tag{2.13}$$

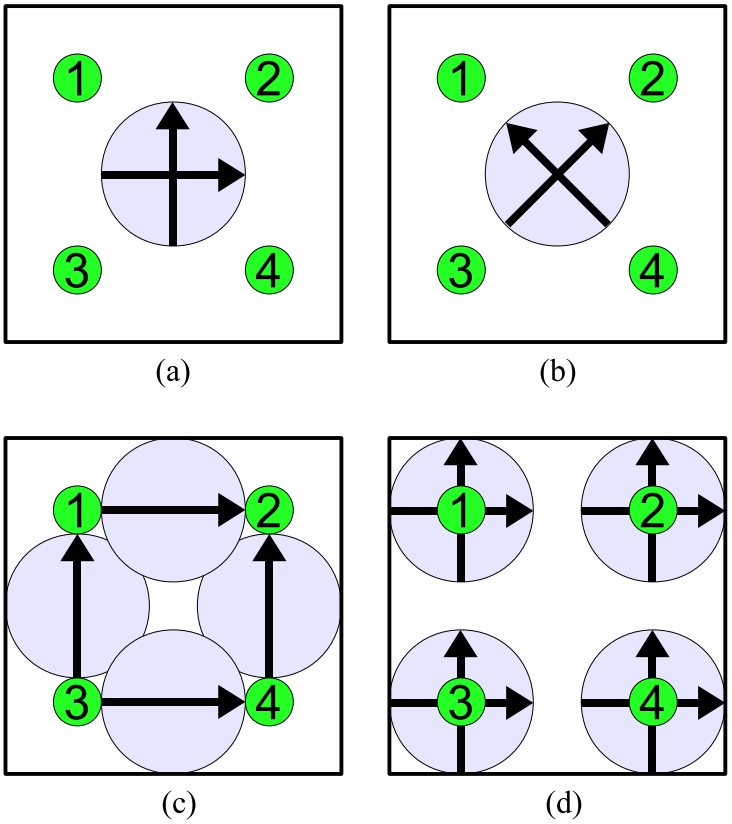

Figure 2.5: Common actuator-WFS geometries: (a) Fried, (b) WCE, (c) Hudgin, (d) Southwell. The numbered circles show the positions of four DM actuators, the light blue circles represent the subapertures measured by the sensor, and the arrows show how the slopes are defined in those subapertures [20].

Because the relationship between phase and actuator position is not unique, the matrix $(\Gamma^T\Gamma)^{-1}$ is often singular and hence non-invertible. In order to prevent the singularity, the piston of the DM, or average actuator position, is set to a fixed value, p. Equation (2.12) can then be written in augmented form as

$$\begin{bmatrix} y \\ p \end{bmatrix} = \begin{bmatrix} \Gamma \\ 1/N \cdots 1/N \end{bmatrix} c \tag{2.14}$$

With this modification, the matrix is now invertible and the phase of the wavefront can be reconstructed from the slope measurements. Other sensors, such as the self-referencing interferometer, which measure the field directly instead of the wavefront slopes, do not require this type of phase reconstruction.

2.1.3.2 Self-Referencing Interferometer. Another type of wavefront sensor, known as a self-referencing interferometer (SRI WFS), directly measures the wavefront field [18]. An SRI WFS works by splitting an incoming optical field into a reference field and a beacon field as depicted in Figure 2.6. The interference pattern resulting from the two beams traveling through equidistant paths can be used to measure the field of the wavefront. This is done by passing the reference field through a single mode fiber. The fiber spatially filters the beam and provides a known field at the output. The reference path also contains an optical amplifier and a phase shifter. The phase shifter controls the phase of the reference and the optical amplifier increases the amplitude of the interference fringes to enhance the measurement accuracy.

If the beacon field is defined as $A_b(x, y)\exp(i\phi_b(x, y))$, and the reference field is defined as $A_r(x, y)$, the intensity of the n-th phase shift at the m-th subaperture center is

$$I_n(x_m, y_m) = \iint_{\mathcal{A}_m} \left[A_b^2(x, y) + A_r^2(x, y) + 2A_b(x, y)A_r(x, y)\cos(\phi_b + \theta_n)\right] dx\, dy \tag{2.15}$$

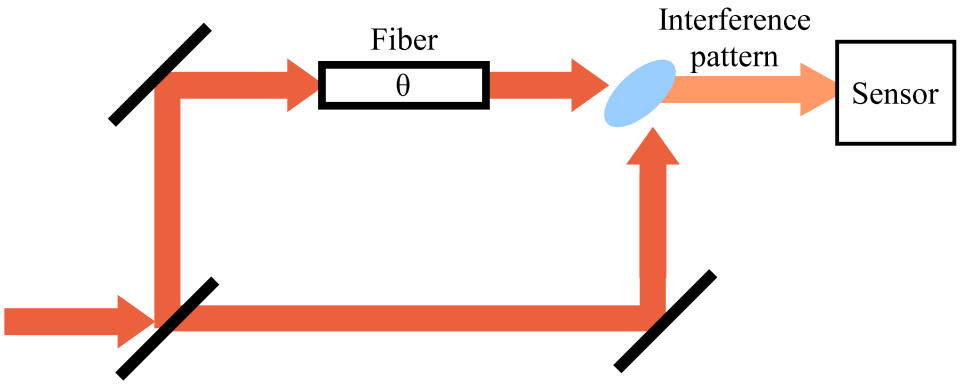

Figure 2.6: Diagram showing how an SRI WFS creates an interference pattern [18].

where θ_n is the phase shift applied to the reference beam and (x_m, y_m) is the position of the subaperture. The integral is performed over the subaperture area, $\mathcal{A}_m$. The unknown beacon field, $U_b(x, y)$, can be estimated from these intensity measurements by using shifts of $\theta_n = [0, \frac{\pi}{2}, \pi, \frac{3\pi}{2}]$. This estimate is,

$$\hat{U}(x_m, y_m) = \frac{1}{4\mathcal{A}_m}\{[I_1(x_m, y_m) - I_3(x_m, y_m)] + i[I_4(x_m, y_m) - I_2(x_m, y_m)]\}$$

The amplitude and phase estimates of the beacon field can easily be computed as

$$\hat{A}_b(x_m, y_m) = \frac{1}{4\mathcal{A}_m}\sqrt{[I_1(x_m, y_m) - I_3(x_m, y_m)]^2 + [I_4(x_m, y_m) - I_2(x_m, y_m)]^2} \tag{2.16}$$

$$\hat{\phi}(x_m, y_m) = \arctan\left[\frac{I_4(x_m, y_m) - I_2(x_m, y_m)}{I_1(x_m, y_m) - I_3(x_m, y_m)}\right] \tag{2.17}$$

In this case, the phase estimate, $\hat{\phi}$, lies between $-\pi$ and π.

An SRI can be designed to apply the four phase shifts in a number of ways. The first method is to use the fiber phase shifter to apply each phase shift temporally. In this case, four successive camera frames are used to create a single SRI measurement. Another method is to divide the reference beam into four separate beams and apply the appropriate phase shift to each beam. The resulting interference intensities can then be imaged simultaneously using either four individual detectors or four regions

of a single detector. It is also possible to use a hybrid approach, which splits the beam into two paths and uses two successive frames from each path to obtain the full set of four interference patterns necessary for a single SRI measurement. There are advantages and disadvantages to both spatial and temporal phase shifting techniques. When using spatial phase shifting, the same beacon field is used for each measurement which is advantageous with rapidly evolving turbulence. However, when using multiple propagation paths for the different beams and different detectors for each interference pattern, proper calibration and alignment become more difficult. Temporal phase shifting avoids these calibration and alignment issues and also provides a higher spatial resolution for a given detector, since it is not necessary to partition the detector array. The drawback to temporal phase shifting is that measurement bandwidth is reduced by a factor of four [18].

With either spatial or temporal phase shifting, the SRI WFS provides a measurement of the wavefront phase. This measurement is used to determine the shape of the DM needed to conjugate the phase of the wavefront. The AO control algorithm describes how the WFS measurement is used to command the DM.

2.1.4 AO Control. Although the DMs used in AO have a large number of actuators, typical controllers operate under the assumption that each actuator is independent and can be controlled as a single-input single-output (SISO) system. Typically, the same control law is used for each actuator, although some research has been done using non-uniform gain controllers [21]. The discrete-time controller used by Barchers is

$$c(n+1) = ac(n) + (1-a)K_{DC}e(n+1) \tag{2.18}$$

where $c(n+1)$ is the next DM command, $c(n)$ is the current mirror command, $e(n)$ is the residual phase measurement and a and K_{DC} are design parameters [3]. The parameter a is known as the integrator gain and K_{DC} is the DC gain of the controller. Equation (2.18) is often simplified by introducing a new parameter, b, known simply

as the gain which is defined as

$$b = (1 - a)K_{DC} \tag{2.19}$$

With this substitution, the AO control law can be written as

$$c(n + 1) = ac(n) + be(n + 1) \tag{2.20}$$

The equation can also be represented by its z transform

$$F(z) = \frac{C(z)}{E(z)} = \frac{bz}{z - a} \tag{2.21}$$

Figure 2.7 shows a diagram of this control law used in a typical AO system which is designed to regulate the residual phase.

2.2 Woofer-Tweeter AO

One type of AO system that differs from the system presented in Section 2.1, is a two mirror system known as woofer-tweeter AO. The simplest woofer-tweeter arrangement replaces the DM in Figure 2.1 with two mirrors in series. One mirror, the woofer, has low bandwidth and large actuator stroke. The other mirror, the tweeter, has high bandwidth and low actuator stroke. The terminology is borrowed from the familiar two-speaker audio system.

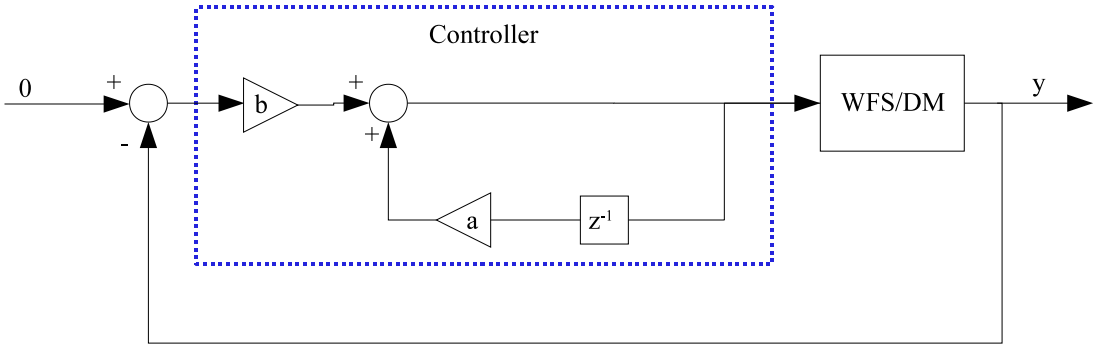

Figure 2.7: Typical AO controller.

2.2.1 Stroke Requirements. In order to understand the need for two mirrors, it is necessary to estimate the actuator stroke requirement of a DM by finding the expected phase variation over the aperture. The maximum phase variation can be found by computing the expected value of

$$\left\langle [\varphi(\mathbf{r}+\mathbf{s}) - \varphi(\mathbf{r})]^2 \right\rangle = 6.88 \left(\frac{|\mathbf{s}|}{r_0}\right)^{5/3} \left[1 - \left(\frac{|\mathbf{s}|}{D}\right)^{1/3}\right] \tag{2.22}$$

over the aperture, where $\varphi(\mathbf{r})$ is the atmospheric phase at spatial coordinate $\mathbf{r}$, and $\mathbf{s}$ is the spatial separation [10]. From this equation, an approximate stroke requirement can be calculated for relatively severe turbulence. The RMS stroke requirement for an aperture of 75 cm, r_0 of 2 cm, and a wavelength of λ is 2.24λ OPD.

To avoid saturation of the DM actuators, the stroke requirement should be about three times the RMS value, or approximately 6.71λ OPD for wavelengths on the order of a micrometer. A high-bandwidth mirror however, typically has a stroke capable of only ± 2 μm OPD and by itself, it is unable to satisfy the stroke requirements [4]. Using two mirrors is one way to achieve the necessary requirement.

2.2.2 Woofer-Tweeter Control. When controlling two mirrors, the typical control approach, described in Section 2.1.4 cannot be used directly. The additional mirror requires that the controller correctly partition the mirror commands between the two DMs. One approach to controlling a woofer-tweeter AO system is to initially present the entire correction to the tweeter mirror controller [4]. The tweeter actuator commands are then directed onto the woofer by means of an off-loading matrix which maps the tweeter commands into corresponding woofer commands. Because the temporal response of the woofer is slower than that of the tweeter, the high-frequency components of the tweeter commands are filtered by the woofer. The net result of the combined off-loading and woofer dynamics is that the woofer corrects for the low-frequency content while the tweeter corrects the high-frequency content.

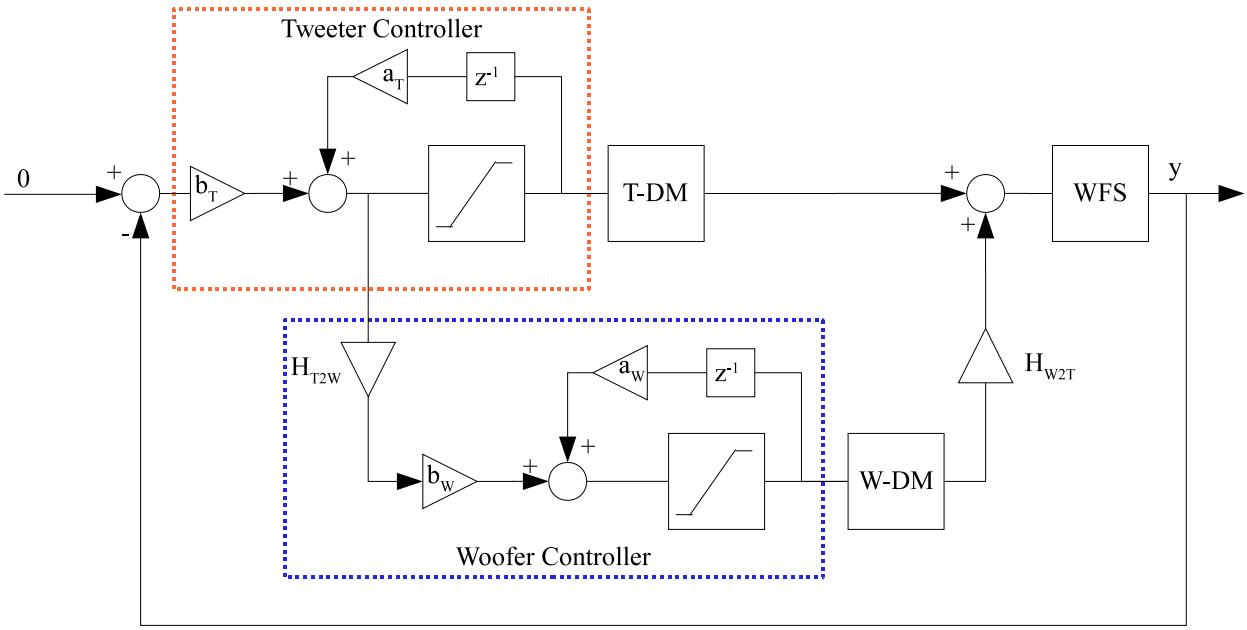

Figure 2.8: Woofer-tweeter AO controller with tweeter commands mapped onto the woofer [4].

Another difference between the woofer and tweeter DM is the spacing of the actuators. The woofer DM has a lower actuator density than the tweeter mirror. Due to the difference in the actuator density between the two mirrors, the tweeter corrects for the high spatial-frequency content while the woofer corrects for the low spatial-frequency content. Figure 2.8 shows a block diagram of this type of control. The offload matrix, H_{T2W}, represents the mapping from the tweeter command to the woofer commands. The addition of the limiters in the block diagram is used to prevent windup of the integrators when the commanded correction exceeds the physical stroke limits of the mirror actuators.

Other methods for controlling a woofer-tweeter AO system use filters to partition the DM commands between the two mirrors [6,7,11]. In these controllers, the response of the woofer mirror is included in the tweeter control loop in order to calculate the appropriate division of DM commands between the woofer and the tweeter mirrors. Thus, the tweeter has two control loops, one for the low-frequency content and one for the high-frequency content.

Regardless of the controller used, the purpose of the woofer-tweeter control algorithm is to allow the dual-mirror system to achieve the performance of a system which uses a high-bandwidth mirror with no stroke limits. Woofer-tweeter control algorithms constitute one of the major components of this research effort. The other major component, adaptive control of AO systems, is discussed in the following section.

2.3 AO and Adaptive Control

Another type of AO system that differs from the traditional approach discussed in Section 2.1 is an AO system which uses an adaptive controller. In a traditional, or fixed-gain controller, the control law is programmed into the control computer and remains fixed throughout the entire operation of the AO system. In many systems, particularly in laboratory environments, an operator can adjust parameters in the control law, such as the constants a and b in Equation (2.20), to achieve the desired performance for a given scenario [3]. However, even when the operator can change the control parameters prior to operating the AO system, they still remain constant while the system is in use. In contrast, an AO system which uses an adaptive controller has algorithms in place to dynamically vary the control parameters in order to consistently achieve the desired performance, without additional tuning by the operator. This section discusses adaptive controllers and their application to AO.

2.3.1 Adaptive Control. While all feedback controllers react or adapt to changes in the environment through the feedback path, they are not necessarily considered adaptive. One definition of an adaptive controller is, "a controller with adjustable parameters and a mechanism for adjusting the parameters" [1]. Because adaptive controller parameters vary in response to the process measurements, they are a form of nonlinear control. Adaptive controllers are most useful in cases where the process dynamics or disturbance characteristics change over time. In such cases, fixed-gain controllers, designed under the assumption that the underlying process is

linear and time-invariant, may not perform adequately. One type of adaptive controller is a model reference adaptive system (MRAS).

2.3.2 Model Reference Adaptive System. A model-reference adaptive system is an adaptive control technique which consists of a model that describes the desired response of the regulated plant, a regulator which controls the plant, and an adjustment mechanism which varies the regulator parameters. The goal of the MRAS system is to adjust the regulator parameters such that the regulated plant has the same behavior as the model. Figure 2.9 shows a block diagram of an MRAS. One approach to designing an MRAS is the gradient method. In the gradient method, the regulator parameters are adjusted in the direction that drives the error between the desired response and the true response to zero.

Åström and Wittenmark outlined the steps of implementing an MRAS using the gradient method [1]. The first step in the gradient method approach is to define a cost function, J, that the controller tries to minimize. Let

$$J(\theta) = \frac{1}{2}e^2 \tag{2.23}$$

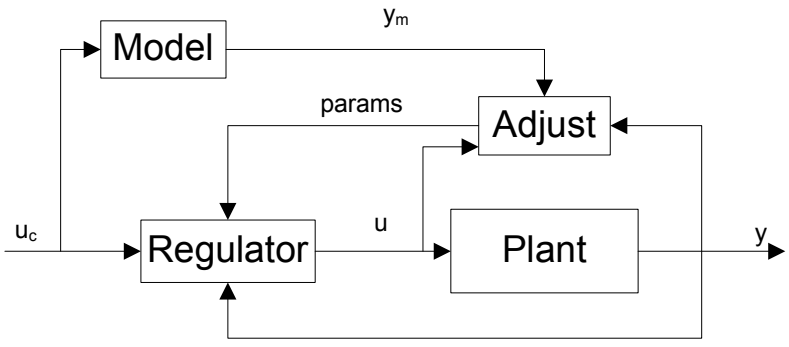

Figure 2.9: Model Reference Adaptive System (MRAS), is a form of adaptive control which finds the regulator parameters necessary to drive the plant such that the closed-loop system behaves like the model system [1].

where θ is the adjustment parameter, and e is the error between the model output, y_m, and the true system output, y. That is,

$$e = y - y_m \tag{2.24}$$

Note that the adjustment parameter θ in this derivation follows standard MRAS notation and is not related to the phase shift described in Section 2.1.3.2. With the cost function and error defined, the parameters are adjusted in the direction of the negative gradient of J in order to minimize the cost. If the parameters of the true system are assumed to be constant, the adjustment of the estimated parameters, θ, can be written as

$$\frac{d\theta}{dt} = -\gamma \frac{\partial J}{\partial \theta} = -\gamma e \frac{\partial e}{\partial \theta} \tag{2.25}$$

where γ is an arbitrary step size. This adjustment rule is known as the MIT rule. By using the MIT rule, the adaptive controller can determine the parameter values necessary to drive the output of the plant to match the desired model response. It is important to note that in the MIT rule the adjustment in Equation (2.25) is proportional to the error, e. This means that parameter convergence slows once the system's performance begins to match the model system. As a result, the parameters may not converge to the true values. However, because the goal of the MRAS is to reduce e, it does not matter, from a control standpoint, whether the parameters have converged. One drawback to the MRAS system described here is the fact that it does not guarantee stability. A poor choice of the parameter γ can lead to instability [1]. This limitation is one of the reasons that lattice filter controllers are also be considered in this research.

2.3.3 Lattice Filter. Another type of adaptive control is a lattice-filter-based approach which has been successfully used in several AO applications [8,9,14–17,19]. The controllers all use a finite impulse response (FIR) lattice filter. FIR filters which have no feedback consist of a weighted sum of delayed input values. This structure

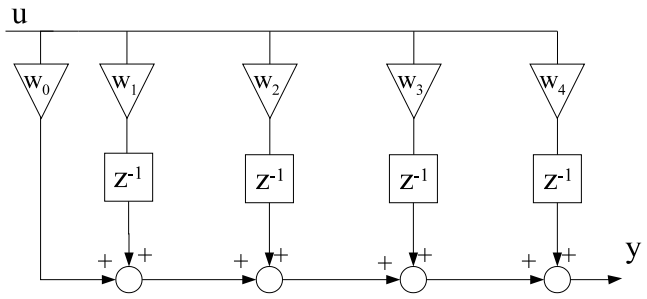

Figure 2.10: Typical structure of a transverse FIR filter.

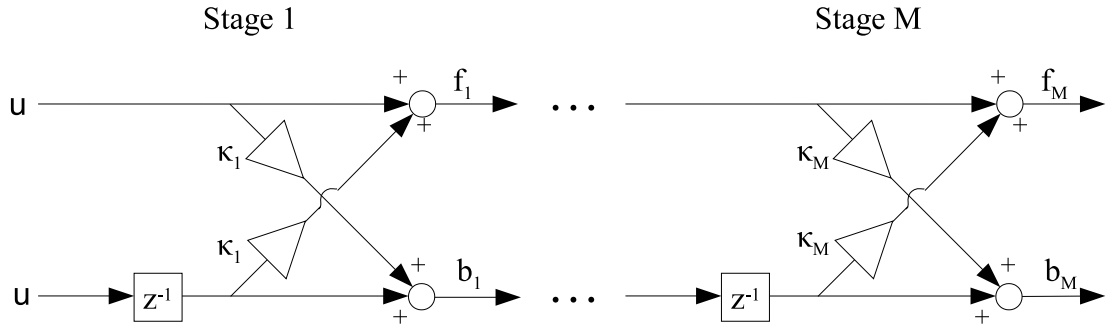

Figure 2.11: A lattice filter consists of a cascade M stages with an identical structure. Each stage is characterized by its reflection coefficient, κ_m. The name lattice filter comes from the lattice-like appearance of the stages.

guarantees bounded-input bounded-output (BIBO) stability. A lattice filter differs from the more familiar transverse FIR filters in form. It can be shown that any given FIR transfer function which can be implemented as a transverse filter can also be implemented as a lattice filter [13]. A transverse FIR filter has the simple structure shown in Figure 2.10. A lattice filter on the other hand, has a more complex structure as shown in Figure 2.11. The name lattice filter refers to the lattice-like appearance of the filter connections. An Mth-order lattice filter consists of M stages with identical structures, with each stage characterized by its reflection coefficient, κ_m. Each stage has two inputs and two outputs that are described by the equations

$$f_m(n) = f_{m-1}(n) + \kappa_m b_{m-1}(n-1) \tag{2.26}$$

and

$$b_m(n) = b_{m-1}(n-1) + \kappa_m f_{m-1}(n) \tag{2.27}$$

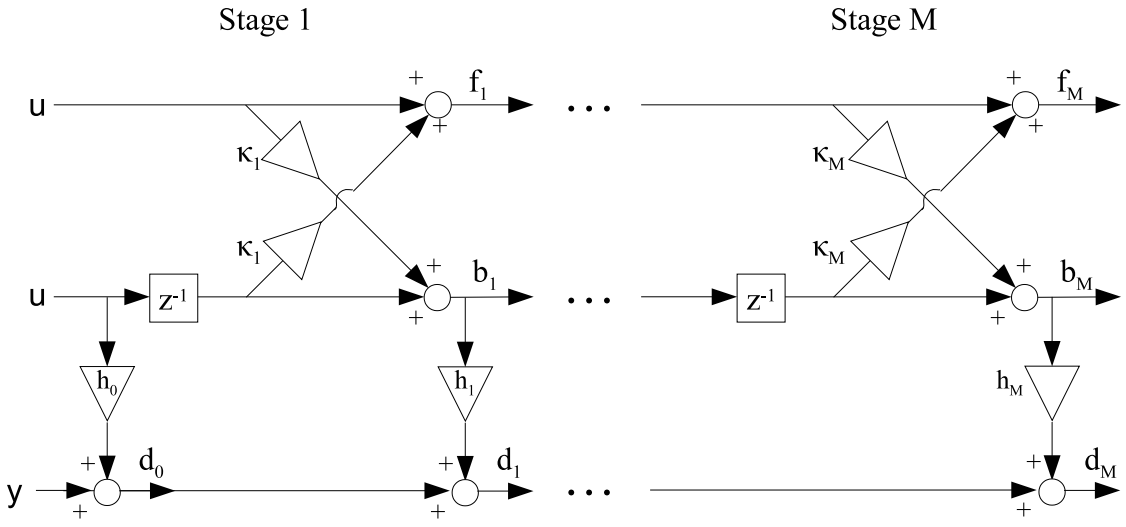

Figure 2.12: A joint-process estimator lattice filter consists of a lattice filter with the addition of weights which operate on the backward prediction errors.

with initial condition

$$f_0(n) = b_0(n) = u(n) \tag{2.28}$$

The quantity $f_m(n)$ is known as the m-th forward prediction error and represents the difference between the input $u(n)$ and the predicted value based on the m previous inputs $u(n-1), \ldots, u(n-m)$. Similarly, the quantity $b_m(n)$ is known as the backward prediction error and is the difference between $u(n-m)$ and the m future inputs $u(n), \ldots, u(n-m+1)$.

By augmenting the structure shown in Figure 2.11 with an additional set of weights, which operate on the backward prediction errors, a lattice filter can be used to predict a correlated sequence. This is known as a joint-process estimator and is shown in Figure 2.12. When the filter input is a correlated stationary process, the backward prediction errors have the important property of being orthogonal. This property of orthogonal prediction errors allows the lattice filter joint-process estimator to adapt faster than a transversal filter because there are no interactions between the filter weights [13]. In addition to faster adaptation, lattice filters are more numerically robust than transversal filters and their modular structure allows the filter order to be increased without affecting previously calculated coefficients [12, 13].

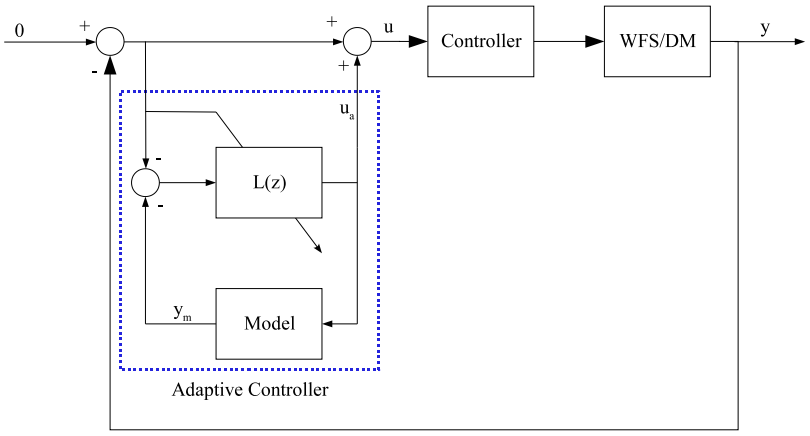

Figure 2.13: Control architecture commonly used in AO controllers which use lattice filters to provide additional input to the traditional fixed-gain controller.

The previously mentioned AO systems with lattice filter adaptive controllers have all used the structure shown in Figure 2.13, with the adaptive controller providing additional input to the fixed-gain controller [8, 9, 14–17]. In the figure, the model is used to provide an estimate of the residual phase measurement, y_m, based on the adaptive controller output, u_a. The signal y_m is used to calculate the error signal, e, between the model system and the true system as in Equation (2.24). This error signal is the input to the lattice filter, $L(z)$. The tuning signal to the lattice filter is the true system output, y. The gains of the lattice filter, $L(z)$, are calculated such that the adaptive control signal, u_a, drives the residual phase measurement, y, to zero.

2.3.4 Modal Control. When dealing with a large number of actuators, the computational burden can become a concern, especially when using complicated algorithms such as adaptive lattice filters. One common method of reducing the computational burden of the controller is to define a set of orthogonal mirror modes and apply the control law to each individual mode instead of each actuator. As long as the number of modes is less than the number of actuators, then the computational burden is decreased. Liu and Gibson defined a modal decomposition that results in orthogonal modes that are ordered according to their spatial-frequency content [15].

This spatial-frequency ordering is useful because it effectively performs lowpass spatial filtering of the DM commands when the higher-order modes are discarded. This can help mitigate high-frequency noise and limit the effects of mis-registration [15]. The process for determining these frequency weighted modes consists of two steps: first finding modes which are orthogonal in actuator-space and then finding modes which are orthogonal in both actuator and sensor-space. In this process the frequency weighting is achieved through the use of a lowpass spatial filter.

The frequency-weighted modal decomposition procedure requires only the actuator geometry and a lowpass filter. The matrices T and S describe the actuator geometry and the matrix F describes the lowpass filter. The columns of T form a set of basis vectors in the space of the master actuators, while S is the slaving matrix that maps the master actuators commands to commands for all actuators. The columns of T can be chosen such that they represent DM shapes with no mean displacement or tilt. If these constraints are not required, T can be the identity matrix. Likewise, if there is no slaving, S can be the identity matrix. F can be the matrix representation of any arbitrary lowpass filter. The frequency-weighted modes are defined as the columns of the matrix

$$V = TX \tag{2.29}$$

where X is the $m \times m$ eigenvector matrix which solves

$$(FST)^*(FST)X = (ST)^*(ST)X\Lambda^2 \tag{2.30}$$

and where Λ^2 is the diagonal matrix of the eigenvalue magnitudes squared, λ_i^2, and * represents the conjugate transpose. If only n modes are needed, then only the first n columns of V are used to define the modes.

The modes described by V are designed to be orthogonal in actuator space and are not, in general, orthogonal in sensor space. In order to find modes that are orthogonal in both actuator and sensor-space, the poke matrix, Γ, which describes the relationship between actuator commands and sensor measurements, is needed. The

new modes are defined as the columns of the matrix

$$\tilde{V} = \Gamma \tilde{X} \tag{2.31}$$

where $\tilde{X}$ is the $n \times n$ eigenvector matrix which solves

$$(\Gamma SV)^*(\Gamma SV)\tilde{X} = (SV)^*(SV)\tilde{X}\tilde{\Lambda}^2 \tag{2.32}$$

Using this method of defining modes, which are orthogonal in both actuator and sensor space, a lattice filter woofer-tweeter controller can now be designed. Building on the material covered in this chapter, Chapter III discusses the design process of both MRAS and lattice filter-based adaptive woofer-tweeter controllers.

III. Simulation Environment and Adaptive Controller Design

This chapter takes the topics in Chapter II and discusses the specific details of how they can be combined to create a new adaptive optics system with improved performance compared to existing approaches. The discussion consists of two parts: the setup of the simulation and the design of the adaptive controllers. The simulation details are presented prior to developing the specific control architectures because some aspects of the design process, such as defining the mirror modes, are dependent on the type of hardware being simulated.

3.1 Simulation

In order to design and test a control algorithm for an adaptive woofer-tweeter AO system it is necessary to have a working simulation of all of the major components of an AO system. As discussed in Section 2.1, these components are the atmospheric turbulence, the DM, the WFS, and the control algorithm. Several commercial software packages exists for simulating these components. Because they were readily available and relatively easy to learn, the MATLAB packages WaveProp and AOTools were used for these simulations [5].

3.1.1 Atmosphere. One way of generating atmospheric turbulence with the desired statistics is to apply a phase screen to a simulated complex optical field. The phase screen adds or subtracts phase from the optical field to simulate the effects of atmosphere on a wavefront. Figure 3.1 shows an example of a phase screen realization using the Kolmogorov turbulence model given in Equation (2.3), with $r_0 = 2$ cm. By applying a phase screen with the appropriate value of r_0 to the complex optical field, it is possible to simulate the desired turbulence to test the adaptive AO controller. While a phase screen provides the correct spatial characteristics of the turbulence, it is also necessary to simulate the temporal variations of the turbulence. Given a wind velocity, V, the corresponding Greenwood frequency, f_G, can be determined

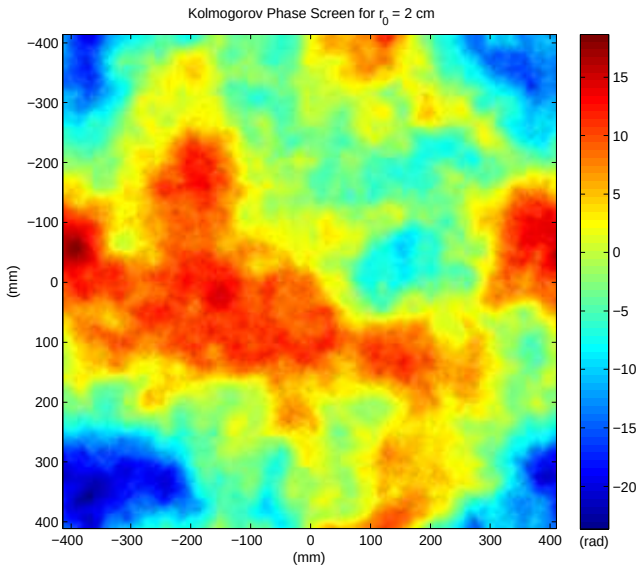

Figure 3.1: An example of a phase screen generated using the Kolmogorov turbulence model with $r_0 = 2$ cm.

from Equation (2.11). To simulate the temporal effects, the phase screen is simply shifted laterally by a distance $V\Delta t$, where Δt is the simulation time step.

Because the focus of this research is to develop an adaptive control algorithm, only a single phase screen is used and all the EM fields are simulated in the pupil plane of the telescope. This approach eliminates the need for additional elements in the simulation, such as telescopes which crop and demagnify the field, and computationally expensive wave propagations which simulate both scintillation of the beacon wavefront and the directed energy performance at the target location. Neither the telescope nor the full-path wave propagations are necessary for demonstrating the feasibility of a new AO control architecture. The inclusion of either the telescope or propagations would not change the design nor implementation of the adaptive control algorithms.

3.1.2 Simulation Parameters. When simulating the performance of the adaptive woofer-tweeter AO system, two different turbulent scenarios are considered. The two scenarios are the same ones used by Brennan and Rhoadarmer [4]. The first

Table 3.1: Simulation Parameters

Parameter	**Low Turbulence**	**High Turbulence**
r_0	6 cm	2 cm
V	20 m/s	20 m/s
f_G	142 Hz	427 Hz

scenario consists of fairly correlated turbulence, which should be easily compensated by the standard fixed-gain AO system. The second scenario consists of less-correlated turbulence which is more challenging for the standard controller. It is expected that the adaptive controller can improve the performance of the AO system in more difficult turbulence while maintaining the performance of the AO system in the case of the lower turbulence. Table 3.1 lists the simulation parameters of the two different scenarios.

3.1.3 Deformable Mirrors. As with the turbulent scenarios, the woofer and tweeter DM specifications are taken from Brennan and Rhoadarmer [4]. Both the woofer and the tweeter DMs are set equal to the simulated aperture size of 76 cm. The tweeter DM has 39 actuators across the aperture with a spacing of 2 cm for a total of 1521 actuators over the square aperture. The woofer DM has 20 actuators across the aperture with a spacing of 4 cm for a total of 400 actuators. To simulate a continuous facesheet DM, the surface of each mirrors is approximated by a bilinear interpolation of its actuator commands. As shown in Figure 3.2, the two mirrors are positioned such that each woofer actuator is aligned with a corresponding tweeter actuator.

In order to simulate a circular aperture, only some of the actuators over the square DM are active. Figure 3.3 shows the layout of the active actuators for both the woofer and the tweeter DMs. The total number of active actuators is 1245 for the tweeter and 316 for the woofer. The alignment shown in Figure 3.2 makes it easy to determine the offloading matrix H_{T2W}. If the active actuators in the 39×39 tweeter grid are represented by a 1245×1 vector and the woofer is similarly represented by

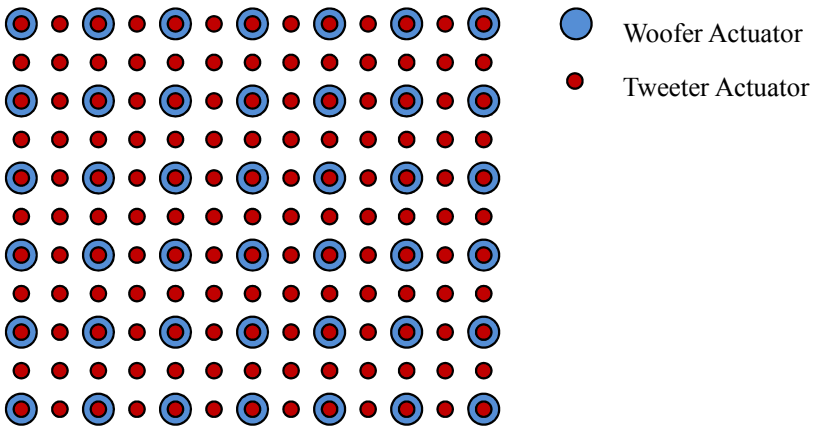

Figure 3.2: Woofer-tweeter actuator alignment. Each woofer actuator corresponds to a tweeter actuator. The spacing between woofer actuators is twice that of the tweeter actuators giving the tweeter a higher spatial resolution. Not all of the actuators are depicted here.

a 316×1 vector, H_{T2W} is a 316×1245 matrix which maps the tweeter actuators to the corresponding woofer actuators. Each tweeter actuator that has a corresponding woofer actuator is represented by a one in the matrix. All other entries in the matrix are zeros. In other words, H_{T2W} effectively down-samples or decimates a vector of tweeter commands to produce the corresponding set of woofer commands. The other matrix, H_{W2T}, is used to determine the effect of the woofer DM at the tweeter DM actuator locations, in order to accurately combine the correction of both mirrors. This matrix is not needed explicitly since it is automatically accounted for in the simulation when the mirror surface is applied to the optical path. If the matrix was needed, it would simply be the matrix representation of a bilinear interpolation of the woofer DM commands to the higher resolution of the tweeter DM commands.

In the simulations, the tweeter DM is assumed to have an infinitely fast response time, compared to the sensor rate, and can be modeled by the transfer function

$$T(z) = 1 \tag{3.1}$$

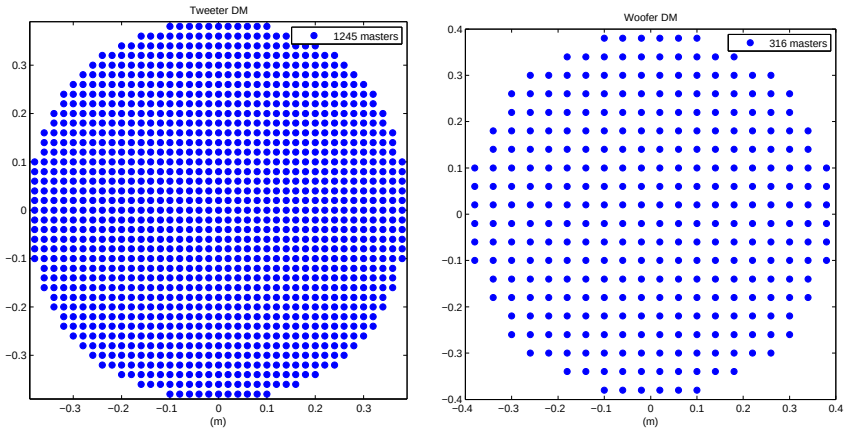

(a) (b)

Figure 3.3: To simulate a circular aperture only some of the actuators are active. The total number of active tweeter actuators is 1245 as shown in (a). The total number of active woofer actuators is 316 as shown in (b).

Table 3.2: Woofer and Tweeter DM Parameters

Parameter	**Tweeter DM**	**Woofer DM**
Integrator gain	$a_T = 0.99$	$a_W = 0.99$
Gain	$b_T = 0.4$	$b_W = 0.1$
Stroke Limit	$L_T = \pm 2.5\mu$m	$L_W = \pm 6.5\mu$m
Subaperture Width	$d_T = 2$ cm	$d_W = 4$ cm

On the other hand, the woofer has a slower response which can be modeled by the transfer function

$$W(z) = \frac{z+1}{2z} \tag{3.2}$$

The tweeter mirror has a maximum stroke limit of $\pm 2.5\mu$m OPD while the woofer DM has a maximum stroke limit of $\pm 6.5\mu$m OPD. Each mirror is driven by the standard controller given by Equation (2.20). For the given mirrors, the optimal values for the control law were determined by Brennan and Rhoadarmer [4]. The values for the control laws, as well as a summary of both DM characteristics are given in Table 3.2. The woofer and tweeter DM gains differ due to the dissimilar temporal responses of the mirrors.

3.1.4 Wavefront Sensor. The wavefront sensor used in the simulations is an SRI WFS with spatially applied phase shifts. Each SRI WFS subaperture corresponds to one tweeter actuator giving a one-to-one correspondence between the SRI WFS measurements and the tweeter DM commands. Because the SRI WFS provides wrapped phase between $-\pi$ and π, a phase unwrapping algorithm is needed. In the simulation software, various phase unwrapping algorithms are available. The common least-squares phase unwrapping algorithm is inadequate in the high turbulence case because the incidence of 2π-phase differences in adjacent subapertures is too great. Instead, the proprietary WaveProp unwrapping function xphase was used to avoid these problems.

3.2 Adaptive Controller Design

The basic approach to designing an adaptive controller for a woofer-tweeter AO system employed in this research is to adaptively control the tweeter mirror only and then transfer the average tweeter commands onto the woofer as described in Section 2.2.2. This approach simplifies the design of the controller, especially when determining the modes for the adaptive lattice filter. With this approach, only the tweeter modes need to be defined, and thus it is not required to find modes that accurately describe two mirrors with different characteristics. In this section, adaptive control of the tweeter DM which is then transferred onto the woofer DM is implemented with both an MRAS controller, as shown in Section 3.2.1, and with a lattice filter-based controller, as shown in Section 3.2.2.

3.2.1 MRAS Controller Design. Because an MRAS controller is relatively simple to both implement and debug, it is used as a preliminary design to verify the feasibility of the general adaptive AO approach. The successful MRAS approach is then implemented using the more complicated lattice-filter-based controller.

One problem that occurs when attempting to use an MRAS with an AO system is that in AO, the commanded input, u_{cmd}, is always zero. As is shown, part of the

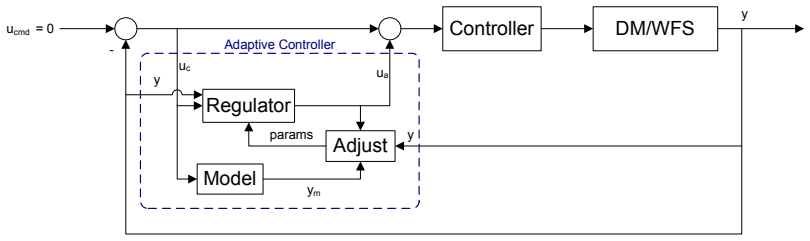

Figure 3.4: MRAS-based adaptive AO control.

parameter adjustment is proportional to u_{cmd}, thus, with no commanded input, the adjustment cannot occur. One way to address this problem is to use the approach employed by Gibson et al. [9,14–16] shown in Figure 2.13. In this approach the adaptive controller is used in addition to the standard fixed-gain controller. The adaptive controller is given the same input as the fixed-gain controller, which is the error signal $u_{cmd} - y$. The controller then creates an additional adaptive control signal, which appears as an additional error to the fixed-gain controller in order to drive the overall system toward the desired response. Although Gibson et al. used a lattice-filter-based adaptive controller instead of an MRAS, the general approach is still the same. Figure 3.4 shows the closed-loop AO system with an MRAS adaptive controller being used in this manner. When implemented in this way, the model system in the MRAS controller is an approximation of the closed-loop transfer function, $Y(z)/U_a(z)$, of the AO system using only the traditional fixed-gain controller. Because the controller is deterministic and known, the MRAS, in effect, attempts to compensate for any modeling errors or non-linearities in the DM and WFS as well as changes in the atmospheric turbulence.

In order to implement the MIT rule as discussed in Section 2.3.2, it is necessary to find the sensitivity derivative, $\partial e/\partial\theta$, from Equation (2.25). The first step in determining the sensitivity derivative is to define the desired, or model, response. Because the desired response of the woofer-tweeter arrangement is to behave like an ideal tweeter with no stroke limits, the woofer is neglected when deriving the model

system for the MRAS controller. The tweeter controller is

$$C_T(z) = \frac{b_T}{z - a_T} \tag{3.3}$$

and the plant consisting of the DM and WFS is

$$P(z) = 1 \tag{3.4}$$

Assuming a unit delay on the feedback path, the MRAS model transfer function is

$$G_m(z) = \frac{-C_T(z)P(z)}{1 + \frac{1}{z}C_T(z)P(z)} = \frac{-b_T z}{z^2 - a_T z + b_T} \tag{3.5}$$

The next step is to find the true system response. Because the true system, $G(z)$, is unknown, it is assumed to have the same form as Equation (3.5) with unknown constants k_1, k_2, and k_3. That is,

$$G(z) = \frac{Y(z)}{U_a(z)} = \frac{-k_1 z}{z^2 - k_2 z + k_3} \tag{3.6}$$

Next, let the output of the MRAS regulator, u_a be defined as

$$u_a(t) = t_0 u_c(t) - s_0 y(t-1) \tag{3.7}$$

where t_0 and s_0 are the adjustment parameters. Substituting Equation (3.7) into Equation (3.6), the transfer function, $H(z)$, from the commanded input to the true plant output is found to be

$$Y(z) = \frac{-k_1 z}{z^2 - k_2 z + k_3}\left(t_0 U_c(z) - s_0 Y(z)\frac{1}{z}\right) \tag{3.8}$$

$$H(z) = \frac{Y(z)}{U_c(z)} = \frac{-k_1 t_0 z}{z^2 - k_2 z + (k_3 - s_0 k_1)} \tag{3.9}$$

Finally, the sensitivity derivatives, $\partial e/\partial t_0$ and $\partial e/\partial s_0$ can be determined from Equation (3.9). Because the model response, y_m, does not depend on the adjustment parameters, t_0 and s_0, it can be ignored when taking the partial derivatives. The sensitivity derivatives are

$$\frac{\partial e}{\partial t_0} = \frac{-k_1 z}{z^2 - k_2 z + (k_3 - s_0 k_1)} U_c(z) \tag{3.10}$$

$$\frac{\partial e}{\partial s_0} = \frac{-t_0 k_1^2 z}{(z^2 - k_2 z + (k_3 - s_0 k_1))^2} U_c(z) \tag{3.11}$$

These equations illustrate the previously mentioned fact that without an input signal, u_c, no adaptation can occur since the sensitivity derivatives are identically zero. The second equation, (3.11), can be simplified and rewritten as a function of $Y(z)$ using the relationship given in Equation (3.9). The simplified sensitivity derivative is

$$\frac{\partial e}{\partial s_0} = \frac{k_1}{z^2 - k_2 z + (k_3 - s_0 k_1)} Y(z) \tag{3.12}$$

Because the parameters of the true system, k_1, k_2, and k_3, are unknown, the adjustment rule cannot be implemented using Equations (3.10) and (3.12). In order to implement the controller it is necessary to make some approximations. The value k_1 appears in the numerator of both derivatives. Because the sign of k_1 is known, it can be incorporated into the arbitrary parameter γ by letting $\tilde{\gamma} = \gamma k_1$. As the parameters converge on their desired values, the denominator approaches that of the desired response, $z^2 - a_T z + b_T$. Thus, the adjustment rule can be based on these desired parameters. With these approximations and by applying Equation (2.25), the parameter update becomes

$$\frac{dt_0}{dt} = \tilde{\gamma} e \left(\frac{z}{z^2 - a_T z + b_T} U_c(z) \right) \tag{3.13}$$

$$\frac{ds_0}{dt} = -\tilde{\gamma} e \left(\frac{1}{z^2 - a_T z + b_T} Y(z) \right) \tag{3.14}$$

In order to implement the MRAS controller with the woofer-tweeter AO system, the adjustment rule was applied to each tweeter actuator independently. In the discrete-time simulation, the sensitivity derivative terms were propagated at each time step using the time domain representation of their transfer function. Both updated parameters, for each actuator, were initialized to one. The parameters were updated by simple Euler integration of Equations (3.13) and (3.14), that is

$$t_0(n) = t_0(n-1) + \frac{dt_0}{dt}\Delta t \tag{3.15}$$

$$s_0(n) = s_0(n-1) + \frac{ds_0}{dt}\Delta t \tag{3.16}$$

where Δt is the simulation time step.

The adaptation parameter, $\tilde{\gamma}$, was set to 10^{15}. While this number seems very large, it is necessary due to the fact that the sampling time is 10^{-4} seconds, the error signal, e, is on the order of 10^{-8} meters, and the command signal, u_c, is on the order of 10^{-7}. If γ is too small, the adaptation occurs too slowly to be of any benefit [1]. With an appropriate step size, the MRAS controller adjusts the controller parameters and drives the AO system to have the desired performance.

3.2.2 Lattice Filter Controller Design. The lattice-filter-based adaptive controller uses the same general control architecture as the MRAS-based controller, with the adaptive controller providing additional input to the fixed-gain controller. Specifically, it used the same structure shown in Figure 2.13 and discussed in Section 2.3.3. Like the MRAS-based controller, the lattice filter-based controller also uses the model transfer function from Equation (3.5). The lattice filter implemented is the gradient adaptive lattice (GAL) filter described by Haykin. The relevant equations are summarized in Equations (3.17)-(3.27) [12]. A more thorough treatment of the GAL can be found Chapter 12 of Haykin's book with prefatory material in Chapters 1, 3, 5, and 6 [12]. The goal of the GAL is to identify the reflection coefficients, κ_m, to minimize

the cost function

$$J_{fb,m} = \frac{1}{2}E[|f_m(n)|^2 + |b_m(n)|^2] \tag{3.17}$$

where $f_m(n)$ and $b_m(n)$ are the forward and backward prediction errors mentioned in Section 2.3.3 and E is the expectation operator. Using Equations (2.26) and (2.27), the derivative of $J_{fb,m}$ with respect to κ_m can be found to be

$$\frac{\partial J_{fb,m}}{\partial \kappa_m} = \kappa_m \left(E[|f_{m-1}(n)|^2] + E[|b_{m-1}(n-1)|^2]\right) + 2E[b_{m-1}(n-1)f_{m-1}(n)] \tag{3.18}$$

Setting the gradient equal to zero and solving for κ_m gives the optimal reflection coefficient

$$\kappa_{m,o} = -\frac{2E[b_{m-1}(n-1)f_{m-1}(n)]}{E[|f_{m-1}(n)|^2 + |b_{m-1}(n-1)|^2]} \tag{3.19}$$

Assuming the process is ergodic, the expectation operator can be replaced by time averages to give the time-varying estimate of the reflection coefficient, $\hat{\kappa}_m(n)$. This estimate, based on time averages, can be written recursively as

$$\hat{\kappa}_m(n) = \hat{\kappa}_m(n-1) - \frac{f_{m-1}(n)b_m(n) + b_{m-1}(n-1)f_m(n)}{\mathcal{E}_{m-1}(n)} \tag{3.20}$$

where $\mathcal{E}_{m-1}(n)$ is the total energy of both prediction errors at time n at the output of stage $m-1$. The total energy is given by

$$\mathcal{E}_{m-1}(n) = \mathcal{E}_{m-1}(n-1) + |f_{m-1}(n)|^2 + |b_{m-1}(n-1)|^2 \tag{3.21}$$

The initial values for Equations (3.20) and (3.21) are $\hat{\kappa}_m(0) = 0$ and $\mathcal{E}_{m-1}(0) = 0$. Equation (3.20) can be rewritten to incorporate a step-size parameter, $\tilde{\mu}$, which leads to faster convergence when the forward and backward prediction errors, and consequently $\mathcal{E}_{m-1}$, are small. The modified equation is

$$\hat{\kappa}_m(n) = \hat{\kappa}_m(n-1) - \frac{\tilde{\mu}}{\mathcal{E}_{m-1}(n)} \frac{f_{m-1}(n)b_m(n) + b_{m-1}(n-1)f_m(n)}{\mathcal{E}_{m-1}(n)} \tag{3.22}$$

Similarly, Equation (3.21) can be modified with the addition of the parameter β to allow for non-stationary environments. The modified equation is

$$\mathcal{E}_{m-1}(n) = \beta\mathcal{E}_{m-1}(n-1) + (1-\beta)\left(|f_{m-1}(n)|^2 + |b_{m-1}(n-1)|^2\right) \tag{3.23}$$

where β is a scalar in the interval $0 < \beta < 1$ and serves to provide a memory of the past value of $\mathcal{E}_{m-1}$ when computing $\hat{\kappa}_m(n)$ [12].

The next part of the GAL algorithm described by Haykin is the desired response or joint-process estimator, which predicts the desired response $\hat{d}_m(n)$ based on the backward prediction errors, that is

$$\begin{aligned}\hat{d}_m(n) &= \sum_{k=0}^{m} \hat{h}_k(n) b_k(n) \\ &= \hat{d}_{m-1}(n) + \hat{h}_m(n) b_m(n)\end{aligned} \tag{3.24}$$

The values of $\hat{h}_m(n)$ are determined using a similar gradient approach that yields the recursive time update equation

$$\hat{h}_m(n+1) = \hat{h}_m(n) + \frac{\tilde{\mu}}{||\mathbf{b}_m(n)||^2} b_m(n) e_m(n) \tag{3.25}$$

where $e_m(n)$ is the estimation error given by

$$e_m(n) = d(n) - \hat{d}_m(n) \tag{3.26}$$

The quantity $\mathbf{b}_m(n)$ is the input vector of the backward prediction errors $b_0(n), b_1(n), \ldots,$ $b_m(n)$, and $\tilde{\mu}$ is the step-size parameter. The Euclidean norm of $\mathbf{b}_m(n)$ can be recursively determined by

$$\begin{aligned}||\mathbf{b}_m(n)||^2 &= \sum_{k=0}^{m} |b_k(n)|^2 \\ &= ||\mathbf{b}_{m-1}(n)||^2 + |b_m(n)|^2\end{aligned} \tag{3.27}$$

Once the lattice filter has been designed according to Equations (3.20)-(3.27), the next step is to determine a set of orthogonal mirror modes. Having the lattice filter operate on a set of orthogonal mirror modes serves to both reduce number of input channels to the filters and allows the filter to adapt to both spatial and temporal variations. When the lattice filter is applied to each actuator independently, it adapts to only the temporal variations at each actuator location. However, when the lattice filter is applied to the orthogonal mirror modes, the filter adapts to the temporal variations of each mode. Because each mode contains spatial information from the entire mirror, as the filter adapts to each mode it is also adapting to spatial variations across all actuators.

The modes were determined using the procedure discussed in Section 2.3.3. In order to determine the modes, it is necessary to define the matrices F, S, and T in Equation (2.30). In these simulations, with no slaving and no constraints on T, both matrices S and T are simply the identity matrix. The matrix F was created using the lowpass filter shown in Figure 3.5. The lowpass filter is the same as the filter used by Liu and Gibson [15]. The filter was generated by creating a one-dimensional eighth-order FIR filter, F_1, with a normalized cutoff frequency of 0.5 using the MATLAB command fir1. A two-dimensional filter, F_2, was created from the one-dimensional filter using the MATLAB command ftrans2, which performs a McClellan transformation. The matrix F is created such that it maps a vector of DM commands to a vector of commands that have been spatially filtered by F_2.

Once the matrices F, S, and T have been defined, the modes can be calculated directly from Equation (2.30). When applying Equation (2.30), it is necessary to sort the resulting eigenvalues in descending order to obtain the correct frequency ordering prior to selecting the n columns of the matrix V which are used in the control algorithm. Naturally, the columns of the eigenvector matrix also need to be sorted to maintain their relationship with the sorted eigenvalues. Because the sensor used is an SRI WFS, where each phase measurement corresponds directly with one actuator, the actuator-space and the sensor-space are identical. This eliminates the need for

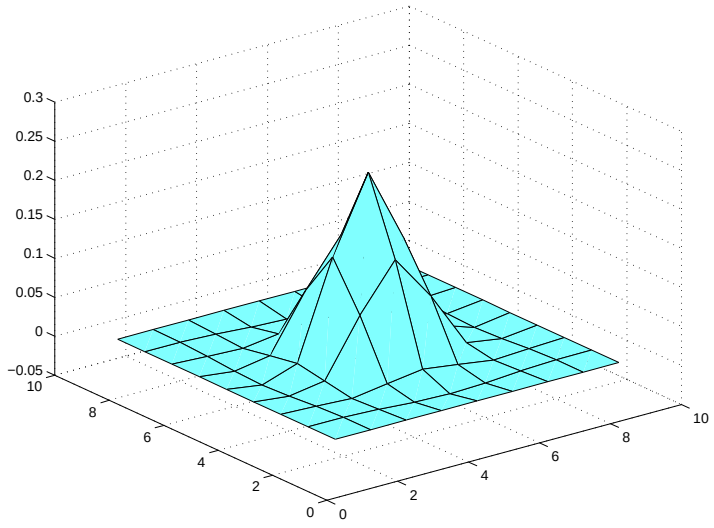

Figure 3.5: Spatial lowpass filter used to determine the DM modes used in the lattice-filer adaptive controller.

applying Equation (2.32), due to the fact that the modes are already orthogonal in both actuator-space and sensor-space. Figure 3.6 depicts the first 24 modes used for these simulations.

Now that the modes have been defined, it is necessary to discuss how the modes are incorporated into the woofer-tweeter control architecture. Because the modes were defined for the tweeter mirror, they can be applied only to the tweeter portion of the control loop. Figure 3.7 shows how this is accomplished. At the input to the adaptive controller, the SRI WFS measurements are multiplied by V^+ to map the phase measurements from actuator space to modal-space, where $^+$ represents the pseudoinverse. Before the adaptive controller output is applied to the traditional controller, it is mapped back into actuator-space by multiplying by V. Thus, the tweeter is controlled adaptively in modal-space while the traditional woofer and tweeter controllers operate in actuator-space as shown in Figure 3.7.

With modes defined and a control architecture which uses them in a woofer-tweeter AO system, the design of the adaptive woofer-tweeter controller is complete. Chapter IV examines the performance of the designed controllers using the simulation

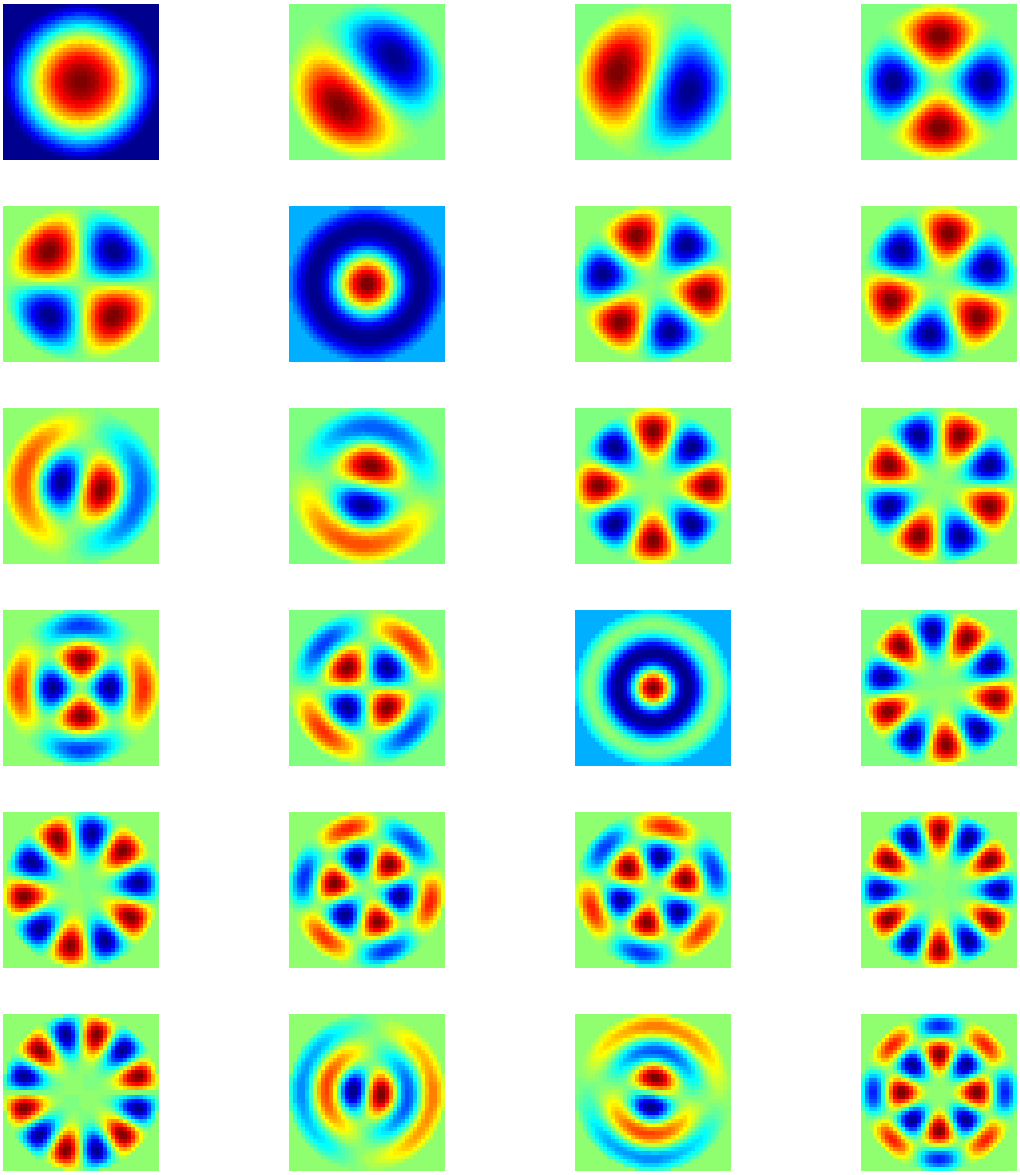

Figure 3.6: First 24 DM modes used in the lattice filter adaptive controller. The modes are orthogonal and ordered according to their spatial-frequency content.

parameters mentioned in this chapter. The controller performance in the simulations is used to determine the appropriate controller settings, such as the lattice filter order and required training time, and to evaluate the design.

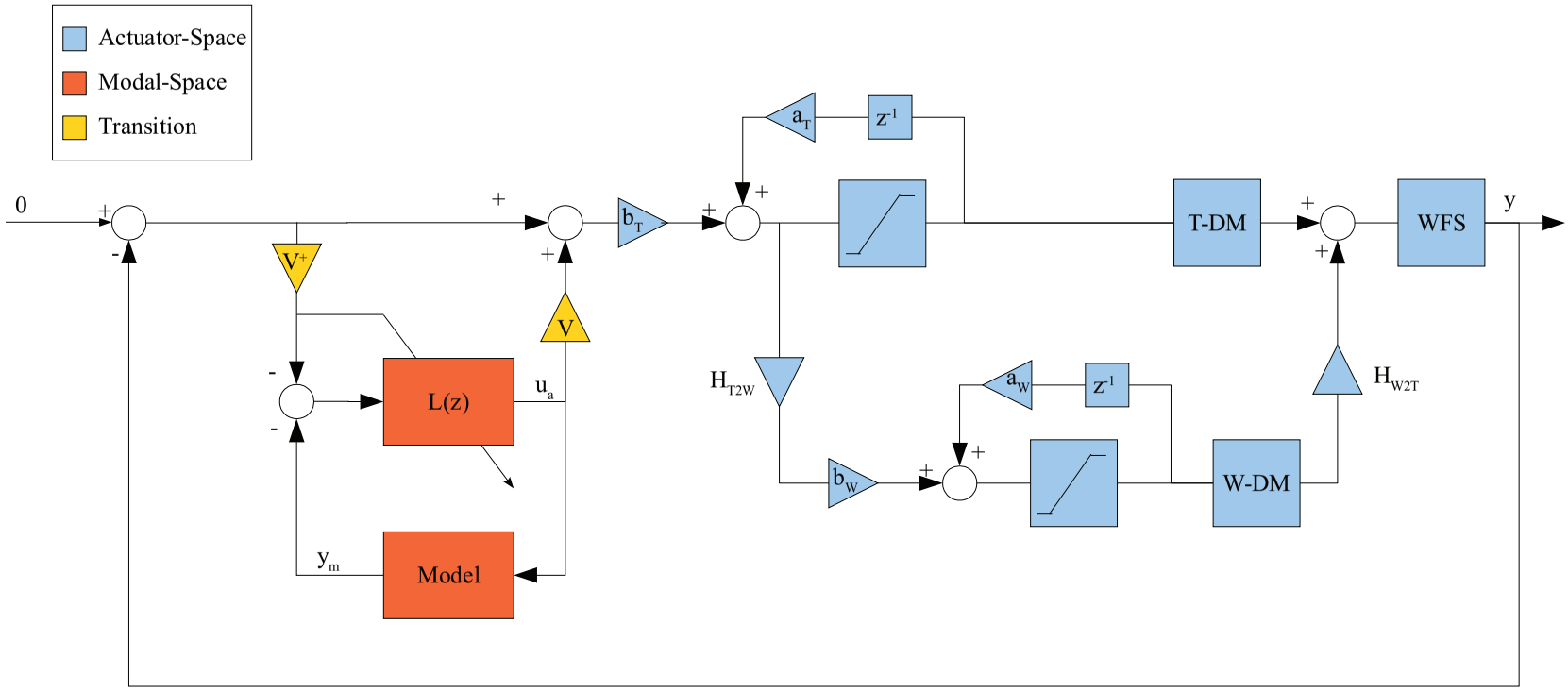

Figure 3.7: Depiction of the control architecture used for modal control of a woofer-tweeter AO system. The adaptive controller operates in modal-space (orange), while the fixed-gain controller operates in actuator-space (blue).

IV. Results and Data Analysis

This chapter presents the simulations of the controllers developed in Chapter III and compares them to a simulation of the fixed-gain woofer-tweeter system. The fixed-gain woofer-tweeter system is simulated first so that a baseline can be established. The other simulations are compared both to the baseline and to each other. The second simulation uses the comparatively simple MRAS controller in order to validate the control architecture of adaptively controlling only the tweeter commands and then transferring them onto the woofer. Lastly, the lattice-filter-based controller is simulated. This lattice filter simulation is broken into two parts: one in actuator-space and one in modal-space. The simulation in actuator-space is used to determine the required training time of the filter and the necessary filter order. The modal-space simulation is then performed using the same training time and filter order. Thus, simulations are presented in order of increasing complexity and are used as stepping stones to the next level of complexity. This approach mirrors the design process that led to the development of the lattice filter controller operating on the system modes.

4.1 Woofer-Tweeter Simulation Results

In order to assess the performance of the adaptive controllers presented in Chapter III, it is necessary to establish a baseline. This was done by simulating a woofer-tweeter AO system that uses traditional fixed-gain controllers. This is the same system which is augmented with the adaptive control loop in subsequent simulations. The first step in ensuring that the woofer-tweeter simulation is working is to verify that the atmospheric correction is being properly partitioned between the two mirrors. Figures 4.1 through 4.3 form a time sequence showing the corrected turbulence, the woofer and tweeter commands used to achieve the correction, as well as the residual phase measurement from the SRI WFS. As seen in Figure 4.1 the initial correction is presented entirely to the tweeter mirror. The woofer initially has no command due to the latency of the transferring procedure. Figure 4.2 shows that after 0.5 ms the

tweeter commands are beginning to be transferred onto the woofer. However, the tweeter is still supplying the majority of the correction as seen by the magnitude of the commands. Figure 4.3 shows that after 2.0 ms the woofer mirror has assumed the majority of the low-spatial-frequency corrections and the tweeter mirror is correcting for the higher-spatial-frequency content.

Another way to visualize the transferring of the tweeter commands onto the woofer is to pick a point in space where both mirrors have an actuator and look at the time history of both actuators at that point. If the woofer-tweeter controller is working properly, the initial correction should be handled exclusively by the tweeter actuator. Over time the woofer actuator should assume the large amplitude low-frequency component while the tweeter actuator corrects only the remaining smaller amplitude high-frequency content. Figure 4.4 shows that this is indeed the case. Furthermore, this figure highlights the need for woofer-tweeter AO since the total correction, shown by the dashed black line, frequently exceeds the tweeter actuator's physical limits of $\pm 2.5 \mu$m.

Figure 4.5 shows the performance of the woofer-tweeter AO system as measured by the Strehl ratio for both the low turbulence and the high turbulence. The average Strehl ratio in the low turbulence case was 0.9063. With the stronger turbulence, the average Strehl ratio drops to 0.4625. For comparison purposes, a single mirror case is shown in which only the tweeter was simulated. As expected, the woofer-tweeter AO system outperforms the single mirror system in both cases. With a single mirror, the average Strehl ratios are 0.8921 and 0.3725 for the low and high turbulence cases, respectively. The large degradation in the single mirror performance in strong turbulence is primarily due to saturation of the tweeter mirror actuators.

4.2 MRAS Simulation Results

With the baseline established, the performance of the different controllers can now be assessed. When the MRAS controller is implemented as shown in Figure 3.4, the injection of the adaptive control signal, u_a, effectively changes the gain of the

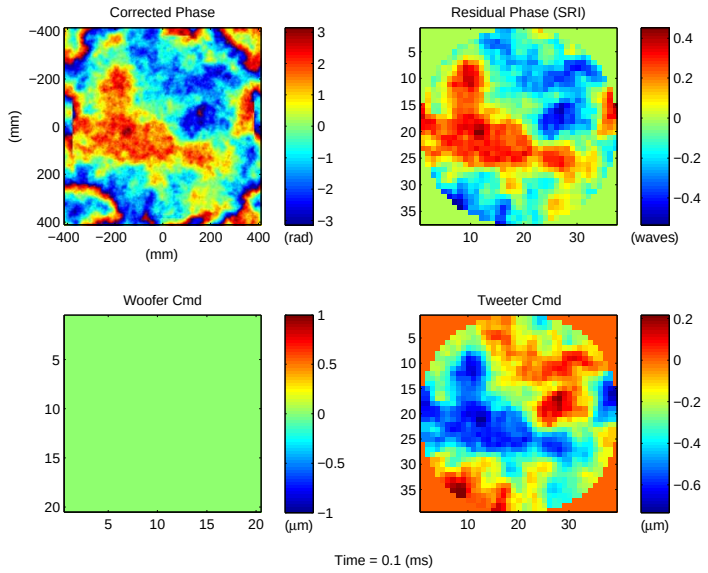

Figure 4.1: The upper-left figure shows the corrected phase of the simulated optical field, while the upper right shows the corresponding SRI measurement. The lower right shows the woofer DM command and the lower left shows that tweeter DM command. Initially the correction is handled exclusively by the tweeter due to the latency in the transfering calculation.

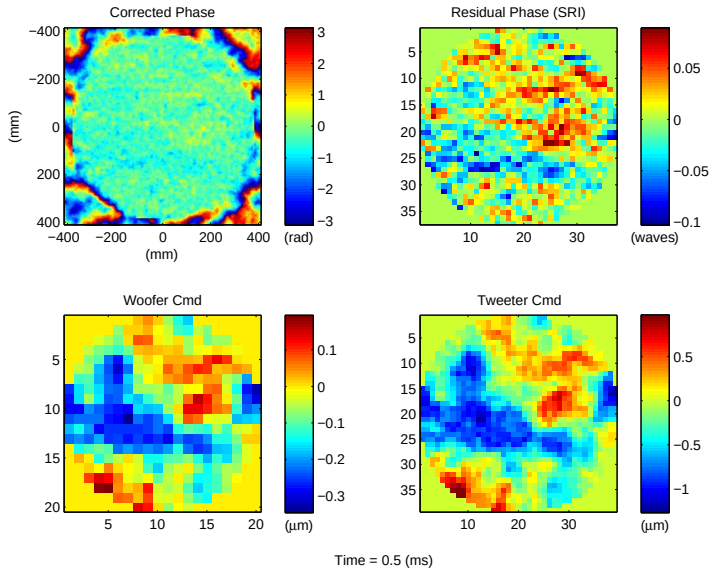

Figure 4.2: After 0.5 ms the tweeter commands are beginning to be transferred onto the woofer. The tweeter is still providing the majority of the correction.

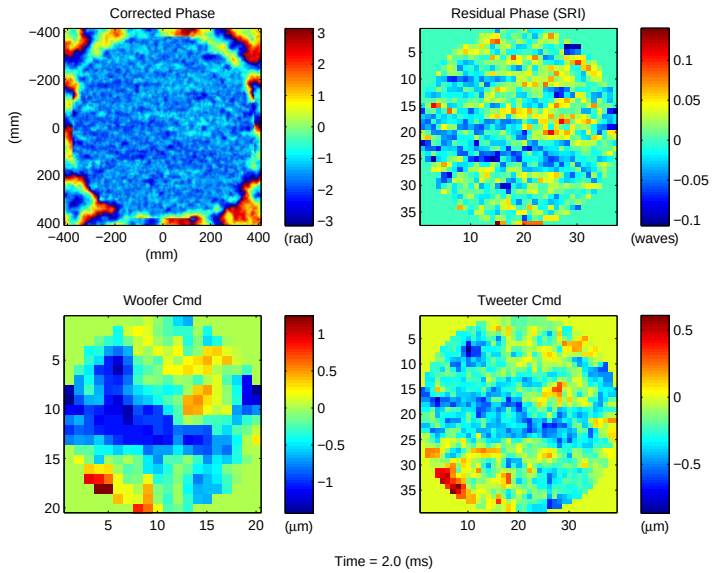

Figure 4.3: After 2.0 ms the woofer is correcting most of the low spatial-frequency components. The remaining high spatial-frequency components are corrected by the tweeter.

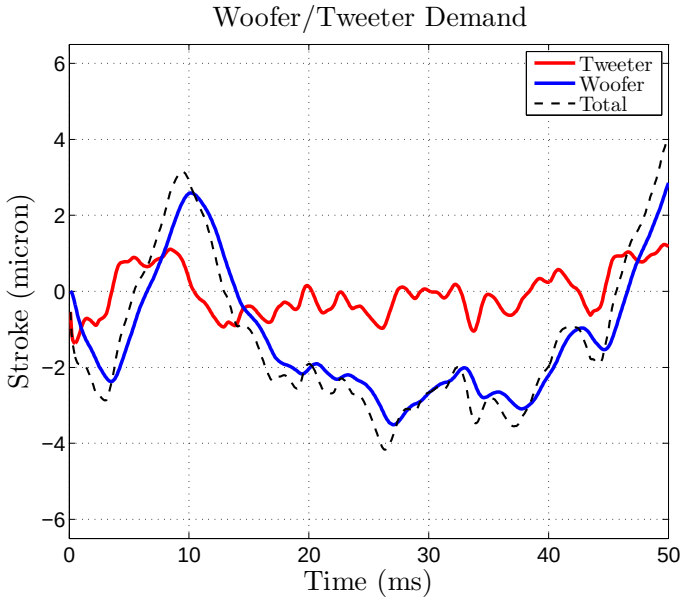

Figure 4.4: This plot shows the history of a woofer actuator and a tweeter actuator that are positioned at the same location in space. The tweeter assumes the low-amplitude, high-frequency corrections and the woofer corrects the large-amplitude, high-frequency content.

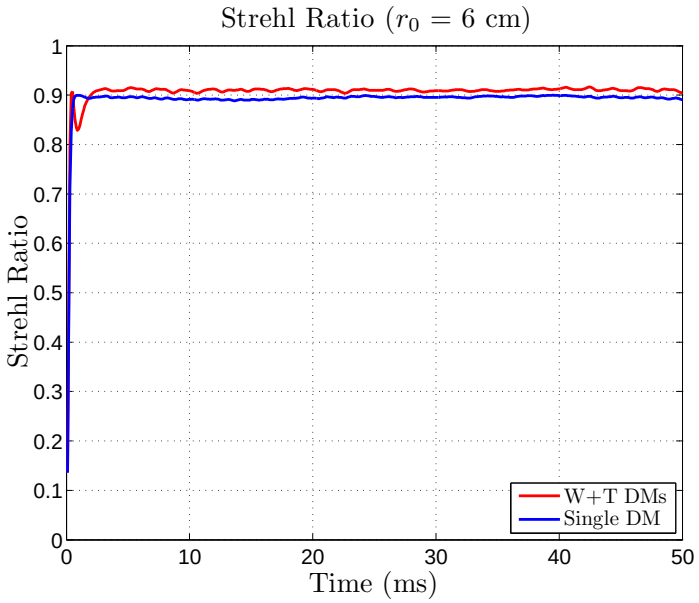

(a)

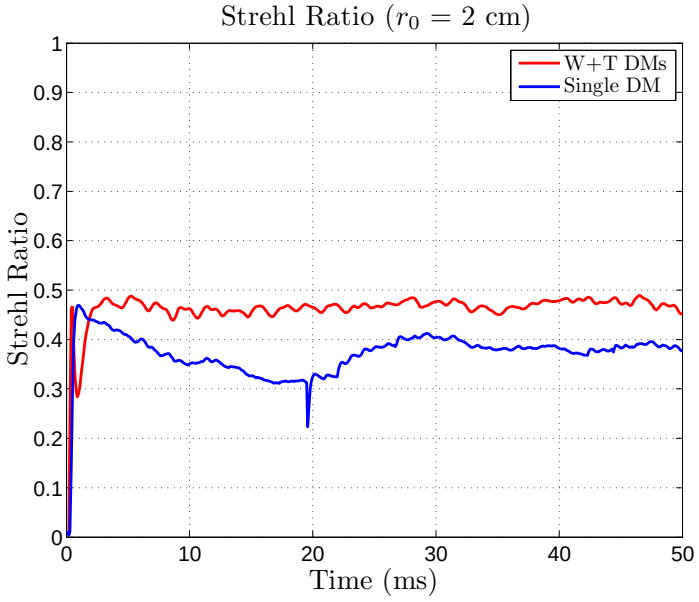

(b)

Figure 4.5: Woofer-tweeter baseline performance in both (a) low turbulence and (b) high turbulence. The red line shows the performance of the woofer-tweeter AO system and the blue line shows the performance of the single mirror system using the tweeter specifications.

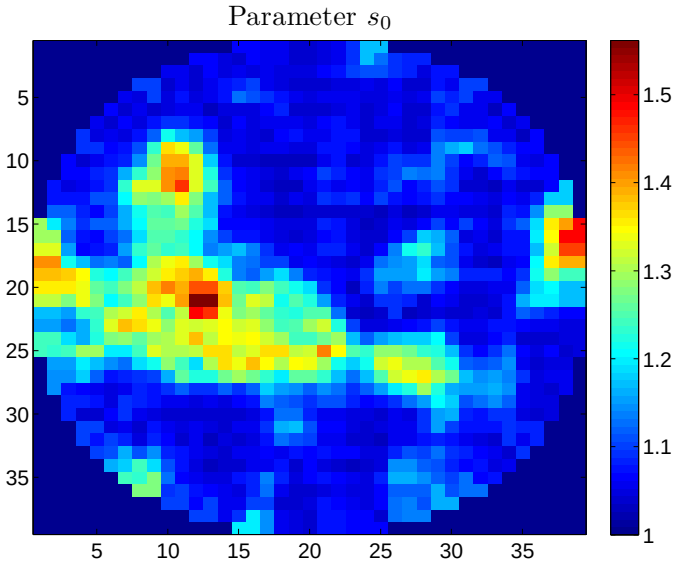

Figure 4.6: Spatial variation of adjustment parameter s_0.

system. Because the adaptive control signal is different for each actuator, the effect of the MRAS adaptive controller is a spatially varying gain on the tweeter. This means that the gain on each actuator varies as the MRAS controller adapts to the deviations from the model. Because the tweeter commands are also transferred on to the woofer as seen in Figure 2.8, the spatially varying control law is represented on the woofer as well. Figure 4.6 shows the spatial variation of the parameter, s_0. The parameter, t_0, also shows a similar pattern. Figure 4.7 shows the time history of the parameter, s_0, for one actuator. The figure suggests that the parameter has not yet converged on its final value even after several iterations. This behavior is expected since the goal of the MRAS is to drive the error to zero, not estimate parameters [1]. Figure 4.8 shows the error between the model response and the response of the actual system for a single actuator. After an initial transient, the output of the AO system essentially matches the desired model output.

Figure 4.9 compares the performance of the MRAS controller with the baseline woofer-tweeter AO system. To allow for a direct comparison, the same turbulence was used in both simulations. To reduce the number of figures, both the high and

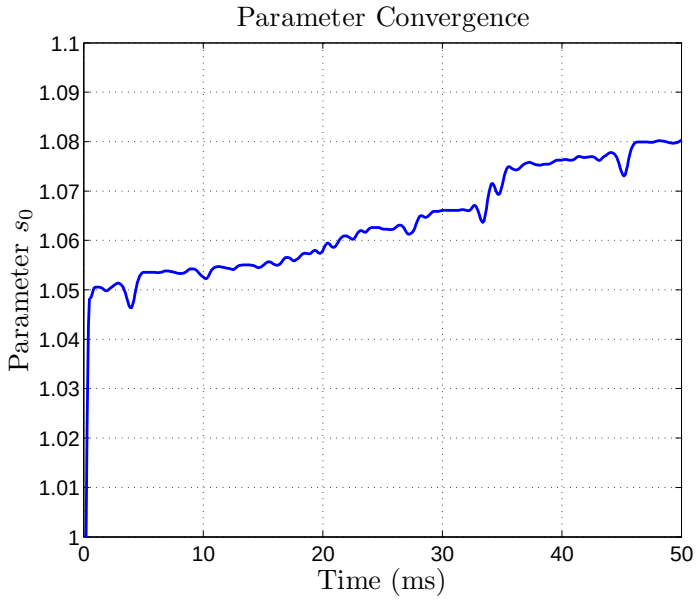

Figure 4.7: Time history of adjustment parameter s_0.

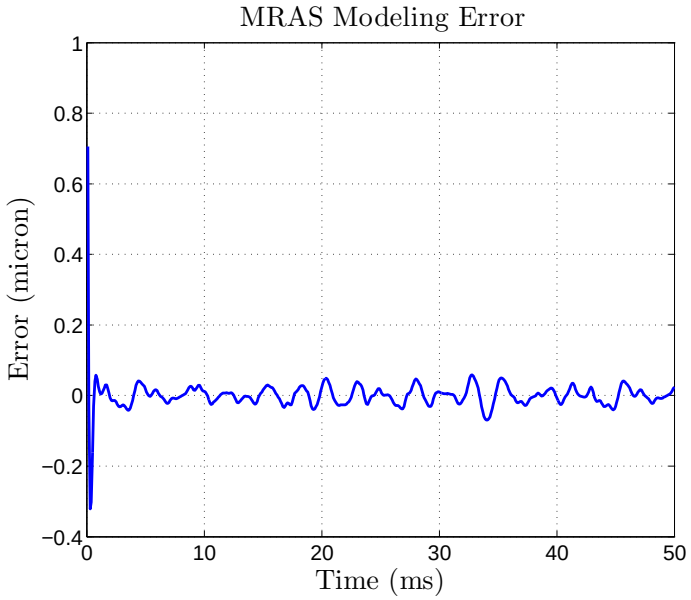

Figure 4.8: The MRAS error, $y - y_m$, measures how well the true system follows the desired model.

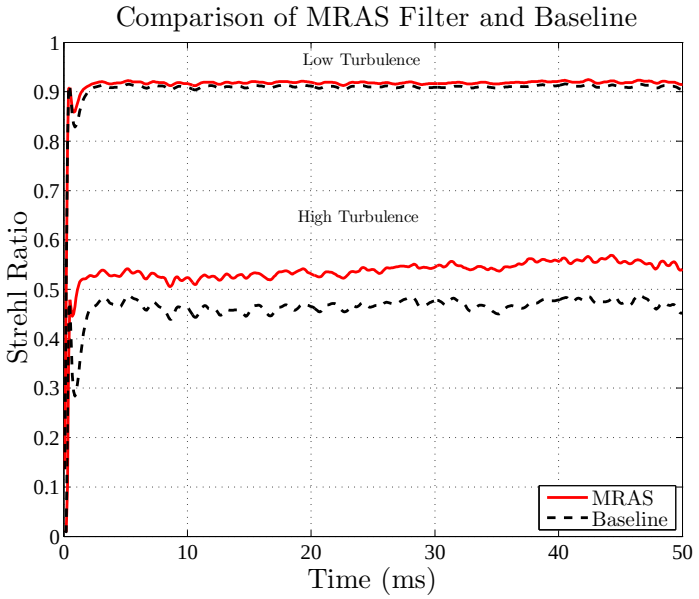

Figure 4.9: Comparison of fixed-gain Woofer-Tweeter AO and MRAS adaptively controlled Woofer-Tweeter.

low turbulence cases are included on the same plot. In the low turbulence, the MRAS controller offers little benefit with an increase in the average Strehl ratio of only 0.009. This increase in the Strehl ratio represents only a 0.94% improvement over the baseline. The small improvement is not surprising due to the fact that the baseline performance is already high and leaves little room for improvement. However, it is encouraging that the adaptive controller provides a benefit even in cases where the traditional fixed-gain controller offers good performance. This result also validates the adaptive control architecture in which only the tweeter is considered. On the other hand, in the presence of the high turbulence the MRAS controller provides significant improvement. The increase in the average Strehl ratio is 0.073, or 15.78%. Also, in both cases the adaptive controller provides the additional benefit of improving the transient performance of the AO system and reduces the initial dip in the Strehl ratio.

4.3 Lattice Filter Simulation Results

4.3.1 Actuator-Space. In order to compare the lattice filter-based controller to the baseline, it is necessary to determine both the number of stages, or order, of

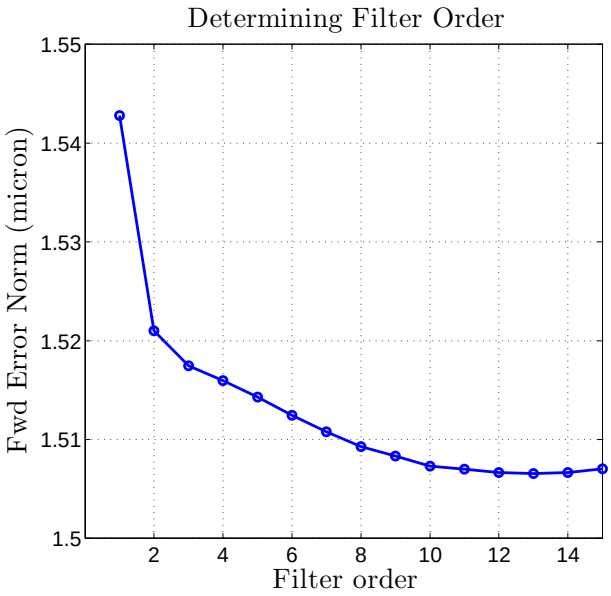

Figure 4.10: The norm of the forward error vector decreases with filter order. The desired filter order can be determined by finding the lowest filter order which still results in a small forward error norm.

the filter as well as the amount of training time required prior to closing the adaptive control loop. The order of the filter was determined using a method discussed by Honig and Messerschmidt [13]. In this method, a vector $\mathbf{F}_m$ is created containing the time history of the forward prediction error at the output of each stage,

$$\mathbf{F}_m = [f(0)_m,\ f(1)_m,\ \ldots, f(n)_m] \tag{4.1}$$

The norm of this forward error vector is then computed for each stage in the filter. As the number of stages increases, the norm of the vector should decrease. The number of stages can be found by observing the norm of the vector and finding when the norm begins to stop decreasing. Figure 4.10 shows a plot of the forward error vector norm as a function of filter order. Using these data it was determined that a filter order of eight represented the lowest filter order desired. Using a lower filter order would result in more error, while using a higher filter order would increase the computational burden of the controller but not significantly reduce the error.

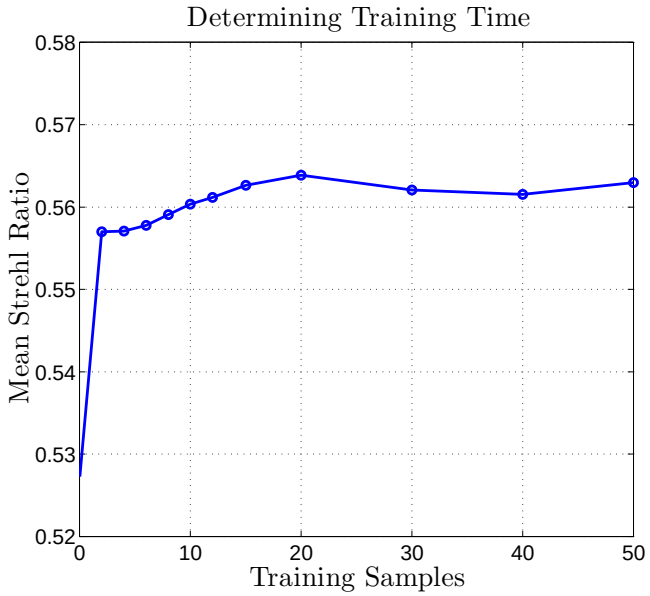

Figure 4.11: The training time for the lattice filter was determined by plotting the mean Strehl for various training times.

In order to determine the best training time for the lattice filter, various training times were used. The mean Strehl ratio for each training time was computed and the best training time was then selected. When calculating the mean Strehl ratio, only the data after closing the adaptive loop were considered. This ensures that only the adaptively controlled portion of the data was considered when measuring the performance. Figure 4.11 shows a plot of the mean Strehl ratio as a function of the number of training samples. Each simulation was run for 100 samples. The training time refers to the number of samples used to train the filter before closing the adaptive control loop. The remaining samples after the training period, when the adaptive controller was active, were used to calculate the mean Strehl ratio. From this plot a training time of 20 samples was selected for the lattice filter controller. When comparing the performance of the lattice filter with that of the fixed-gain and MRAS controllers, two Strehl ratios are computed; the first includes all of the data samples, and the other includes only those that occur after training. Excluding the samples that occur prior to completing the training focuses on the performance gained only when using the adaptive controller. However, the fact that the filter needs to

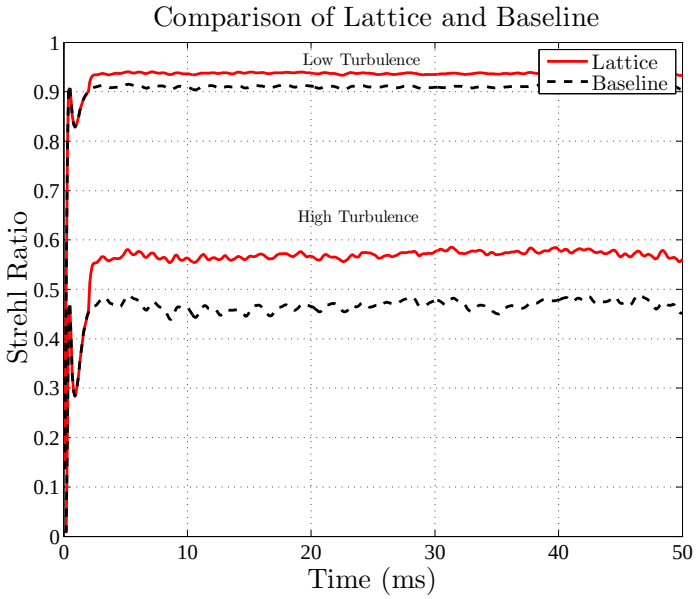

Figure 4.12: Comparison of lattice filter to baseline.

be trained should not be ignored. Averaging over all of the data samples, including those when the adaptive controller is not active, incorporates the training period into the performance metric. Of course, as the number of data samples increases, the low performance during the training period becomes less significant.

With the filter order specified and the number of training samples determined, the performance of the lattice filter controller can be evaluated. Figure 4.12 compares the lattice filter controller to the fixed-gain controller. Prior to completion of training, the lattice filter controller exhibits identical performance to the baseline fixed-gain system because without the adaptive control loop closed, only the fixed-gain controller is active. As with the MRAS controller, the lattice filter controller provides little performance improvement when correcting for the lower turbulence. Again, this is due to the fact that there is little room for improvement over the fixed-gain controller. The improvement in mean Strehl ratio over the entire data sample was 0.025, or 2.86%. When only the active period of the controller is considered the mean Strehl ratio improved by 0.027 for a 2.9% improvement. However, in cases of more severe turbulence, the performance improves dramatically when the adaptive controller loop

is enabled. Immediately prior to closing the adaptive control loop the Strehl ratio was 0.454. After closing the loop, the Strehl ratio rapidly increases to 0.55. The average Strehl ratio over all the data improved by 0.098, or 21.1%. After the training period the improvement was 0.102, or 21.8%.

Like the MRAS controller, the lattice filter controller also exhibits spatially varying gain parameters. Both the reflection coefficients and the joint-process parameters vary spatially. Figure 4.13 shows the spatial variation of the first reflection coefficient, κ_1. No direct comparison of the lattice filter controller parameters and the MRAS controller parameters can be made due to the vastly different structure of the two systems. Still, in both cases the spatially varying parameters equate to a spatially varying control law which adapts to both the turbulence and any un-modeled effects of the DM and WFS. For both the MRAS and the actuator-space lattice filter, this adaptation occurs for each actuator based on its time history. Figure 4.14 shows the time history of the parameter, κ_1, for one actuator. After an initial transient, the parameter converges toward a steady-state value and then fluctuates around that value. This is different than the MRAS controller where the parameters do not reach their steady state values. The error signal, $y - y_m$, measures how well the true system follows the desired model. In the lattice filter controller, this signal is the input to the lattice filter. Figure 4.15 shows a plot of the the error signal at one actuator location.

4.3.2 Modal-Space. Thus far, the lattice filter controller requires the estimation of two parameters for each stage: the reflection coefficient, κ_m, as well as the joint-process weight, h_m. If M is the number of filter stages and N_T is the total number of tweeter actuators, the total number of parameters, N_P, estimated by the filter is

$$N_P = 2MN_T. \tag{4.2}$$

In this case, with 1,245 active tweeter actuators and 8 stages, the total number of filter parameters is 19,920. In comparison, the MRAS controller requires the estimation of only two parameters, s_0 and t_0, for each actuator. This gives a total of only

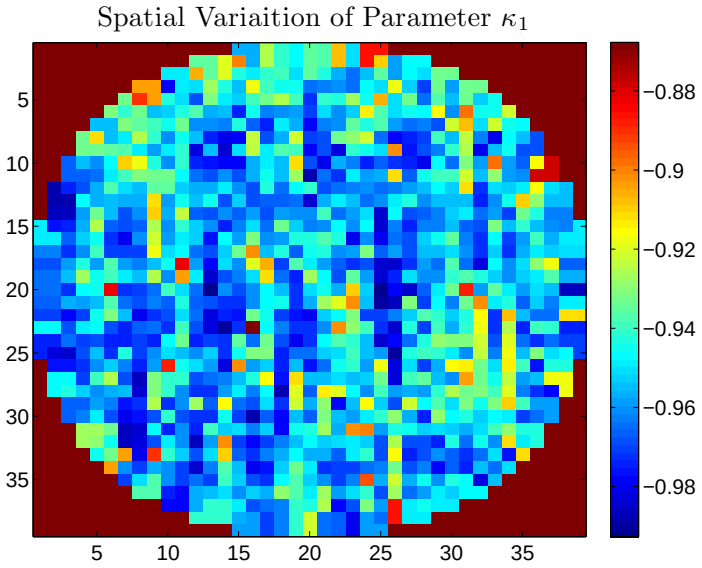

Figure 4.13: The spatial variation of parameter κ_1 at each tweeter actuator.

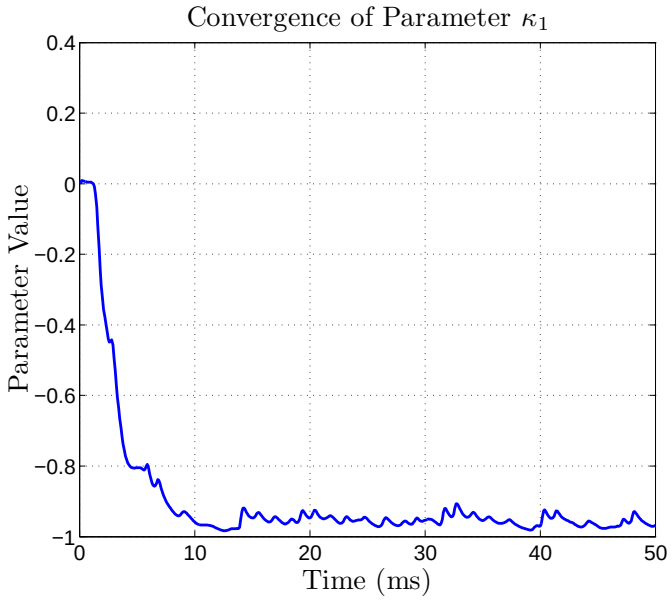

Figure 4.14: The time history of parameter κ_1 for one actuator demonstates how the lattice filter parameters converge over time.

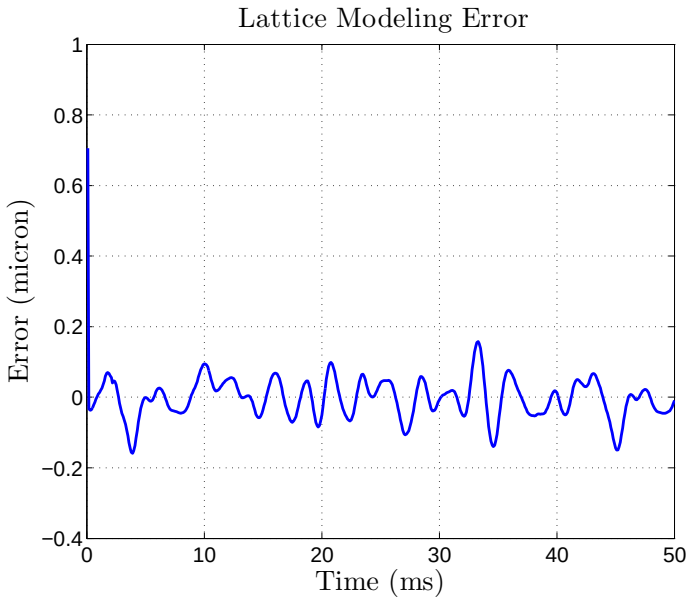

Figure 4.15: The error signal, $y - y_m$, measures how well the true system follows the desired model. This signal is the input to the lattice filter.

2,490 parameters, or one eighth that of the lattice filter. The total number of modes computed in the lattice filter design of Section 3.2.2 is equal to the number of tweeter actuators. Selecting a subset of the modes to control reduces the number of parameters and the computational burden. Figure 4.16 shows a plot of the mean Strehl ratio as a function of the number of modes. It should be noted that in order to shorten the length of the simulation, only 50 time steps were used to generate the plot in Figure 4.16. Because the simulation time was shorter than the other simulations, no comparison should be made between this plot and the performance of the other controllers. The purpose of the plot is simply to identify the minimum number of modes necessary to still achieve a high level of performance. Based on these data, 800 modes were selected for the modal-space lattice filter controller. Using 800 modes reduces the number of parameters by 36%, from 19,920 to 12,800. Figure 4.17 compares the performance of the modal-space lattice filter controller to the baseline case. As expected, the improvement in the low turbulence scenario is minimal with an improvement of only 2% in the mean Strehl ratio. In the high turbulence scenario the improvement is

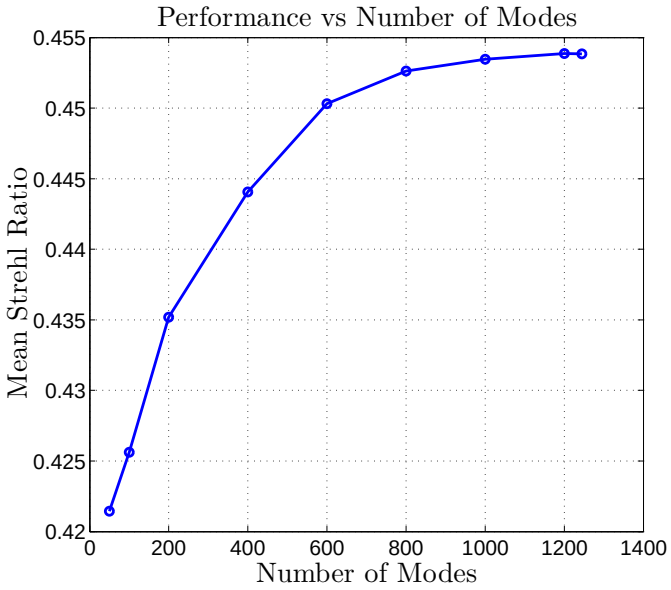

Figure 4.16: Performance versus number of modes

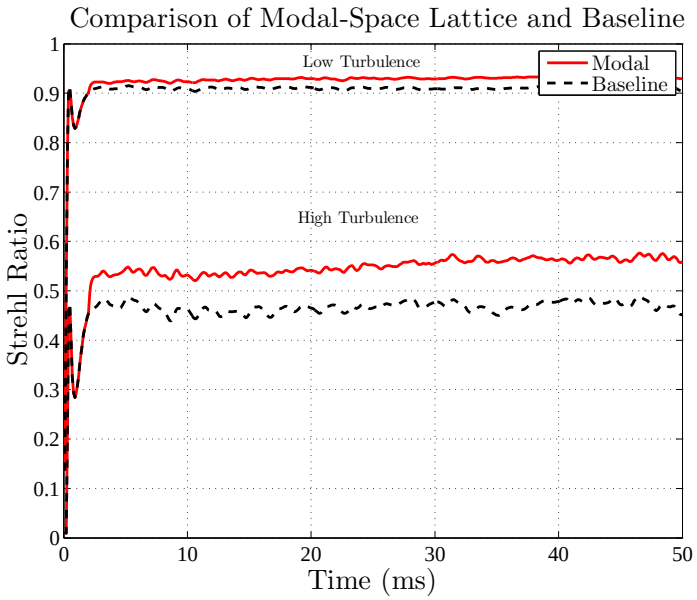

Figure 4.17: Comparison of modal-space to baseline.

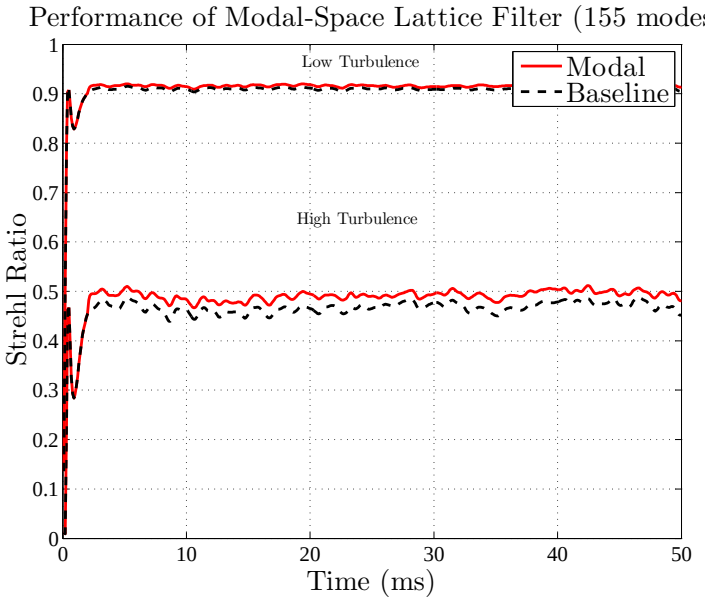

Figure 4.18: Modal-space performance with 155 modes.

17.1%. This performance is more than the MRAS controller, but slightly less than the actuator-space controller using the lattice filter approach. The results suggest that there is a tradeoff between performance and computational burden. To illustrate this tradeoff, the number of modes in the lattice filter is further reduced so the total number of lattice filter parameters is the same as the number of MRAS parameters. Setting $N_P = 2490$ and solving Equation 4.2 for N_T, the required number of modes is found to be 155. Figure 4.18 compares the performance of the modal-space controller with the reduced number of modes. While the performance still exceeds that of the baseline system, the improvement is substantially less. The mean Strehl ratio improved by only 0.67% and 4.98% for the weak and strong turbulent cases, respectively. This represents roughly one third the improvement seen by the other controllers, showing that the lattice filter performance degrades when fewer modes are used. It also shows that when the lattice filter uses the same number of parameters as the MRAS controller, much of the performance improvement is lost and the lattice filter controller no longer outperforms the MRAS controller. The degradation in the lattice filter controller performance is due to the fact that with fewer modes more information is being discarded by the adaptive controller. This implies that if the controller has a limited

computational ability, the MRAS controller can result in better performance than the lattice filter controller, due to the fact that the MRAS controller does not discard information.

With the simulation of the different controllers, it is clear that in all of the cases examined that adaptive control improves the performance of woofer-tweeter AO systems. Chapter V provides a brief summary of the results presented here and gives recommendations for future research on the topic of adaptive control for woofer-tweeter AO.

V. Conclusions and Recommendations

This chapter summarizes the research effort in adaptive control of woofer-tweeter AO and the simulation results presented in Chapter IV. The results are used to provide recommendations for further research. These recommendations aim to further develop the control algorithms presented and extend them to other research areas of interest to the AO community.

5.1 Summary and Conclusion

The goal of this research was to develop an adaptive control algorithm for a woofer-tweeter AO system and to verify its performance with wave-optics simulations. The purpose of the adaptive controller was to improve AO performance, particularly in the presence of high-variance, fast-moving turbulence.

The first step in the design process was to determine a general control architecture for implementing the adaptive controller. Based on recent work by Gibson et al. [8,9,14–17,19], a control architecture where the adaptive controller provides additional input to the standard fixed-gain controller was used. This control architecture was adapted to a woofer-tweeter AO system by applying the adaptive controls only to the tweeter and then transferring the average tweeter commands to the woofer. Using this control architecture, three different adaptive controllers were developed: a model reference adaptive system controller, a lattice filter controller operating in actuator-space, and a lattice filter controller operating in modal-space. The comparatively simple MRAS controller was used to validate the general control architecture. The lattice filter controllers were developed to overcome the potential instabilities inherent in MRAS controllers. A modal decomposition of the DM commands was introduced to both reduce the number of filter parameters and allow the filter to adapt to both spatial and temporal variations in the system.

After designing the controllers, they were simulated in two different scenarios, one with high and one with low turbulence, to measure their performance. A tradi-

Table 5.1: Summary of Results: For each turbulence scenario and each controller type, the number of adaptation parameters, average Strehl ratio, and percentage change from the baseline Strehl ratio are shown.

Scenario	**Controller**	N_P	**Strehl**	**% Change**
Low Turb	Fixed-Gain	0	0.9063	-
	MRAS	2,490	0.9148	0.94%
	Lattice (Actuator-Space)	19,920	0.9370	2.83%
	Lattice (800 Modes)	12,800	0.9245	2.00%
	Lattice (155 Modes)	2,480	0.9124	0.67%
High Turb	Fixed-Gain	0	0.4625	-
	MRAS	2,490	0.5355	15.78%
	Lattice (Actuator-Space)	19,920	0.5602	21.13%
	Lattice (800 Modes)	12,800	0.5416	17.10%
	Lattice (155 Modes)	2,480	0.4855	4.98%

tional fixed-gain controller was used as the baseline case for each scenario. Table 5.1 summarizes the simulation results for each of the adaptive controllers used.

In the low turbulence scenario, none of the adaptive controllers resulted in a substantial performance increase. The actuator-space lattice filter controller, which resulted in the most improvement, only increased the average Strehl ratio by 2.8%. These small gains in low turbulence are due to the fact that the overall AO performance is already high and does not leave much room for improvement. However, in all cases the adaptive controllers improved the performance of the woofer-tweeter AO system.

The simulation results in the high turbulence scenario demonstrate the performance differences between the various adaptive controllers. Again, the actuator-space lattice filter controller showed the most improvement, with a 21% increase in the average Strehl ratio. This performance comes with a computational burden of nearly 20,000 filter parameters. If the number of parameters is reduced by roughly 30%, through the use of a modal decomposition, the average Strehl ratio still increases by 17%. If, however, the number of lattice filter parameters is further reduced to be equal to the number of MRAS parameters, the modal-space lattice filter controller

only increases the average Strehl ratio by 5%, while the MRAS controller acheives a 17% improvement with the same number of parameters.

In summary, the actuator-space lattice filter adaptive controller results in the most improvement in AO performance, in both low and high turbulence. This performance comes at a relatively large computational cost as measured by the number of filter parameters required. If a similar number of parameters are used in both the lattice filter and the MRAS controllers, the MRAS controller results in better performance. However, the MRAS controller does not guarantee stability. A poorly chosen step size parameter, γ, could possibly lead to instability. The lattice filter, on the other hand, with a FIR implementation, guarantees BIBO stability and has no arbitrary parameters that can affect stability. For these reasons, the modal-space lattice filter controller with 800 modes is the best controller for the scenarios presented. It offers good performance, guaranteed stability, and a lower number of filter parameters. In practice, each AO system is unique and none of the presented controllers can be considered superior to the others in all cases. In fact, if only a limited amount of computational resources are available, the MRAS controller would be a reasonable choice.

5.2 Recommendations

Several alternatives exist for implementing or improving upon the adaptive control algorithms presented. This section discusses some of these areas of possible future research.

The results presented in this research were all based solely on computer simulations. Perhaps, the most logical extension of this research is to implement and test the controller designs using real hardware. In any simulation it is impossible to fully capture the intricacies of the real world. With real devices, though, all un-modeled effects are unavoidably included and it is possible to obtain a true measure of the system performance. Prior to implementing the adaptive controller with real hardware it is possible to predict the average improvement and standard deviation of a

given controller using Monte Carlo simulations using different atmospheric turbulence seeds.

Another possible area of future research would be to implement the controller with more complicated systems. As mentioned briefly in Chapter II, some recent work has been done using spatially varying fixed-gain controllers [21]. If a spatially-varying gain were used on the fixed-gain controller, these same gains would need to be incorporated into the system model used in the adaptive controllers. While this change may be fairly straightforward in the controllers which operate in actuator space, research would have to be done on how to map the spatially varying gain into the modal-space model. It is conceivable that such research could yield an adaptive control law where the gains of the model system vary by mode instead of modelling each mode identically.

Another possibility would be to investigate the contribution of each mode over time. If certain modes are found to be more significant sources of error, it might be possible to design an adaptive controller which applies itself only to the significant modes. Such a controller might be able to maintain a high level of performance with fewer adaptive parameters by dynamically selecting which modes to control.

The last recommendation primarily relates to fixed-gain woofer-tweeter AO. It is possible that using an offloading technique other than simply downsampling the tweeter command, might change the performance of the woofer-tweeter AO system. An example of how this might be done would be to generate the woofer commands based on an weighted average of the adjacent tweeter commands by creating a filtered version of H_{T2W}. Since the offload matrix did not factor into the design of the adaptive controllers, this change would not effect the design of the adaptive controller.

These recommendations represent only a few of the areas where future research can be conducted. There are likely several possible areas of research that have not been considered here. Given the demonstrated benefits of adaptive control to woofer-tweeter AO systems, further research in the area is encouraged.

Bibliography

1. Åström, Karl Johan and Björn Wittenmark. *Adaptive Control*. Addison-Wesley, 1989.

2. Andrews, Larry C. and Ronald L. Phillips. *Laser Beam Propagation through Random Media*. SPIE Press, Bellingham WA, 2nd edition, 2005.

3. Barchers, Jeffery D. *Higher order control laws for adaptive optical systems*. Technical Report AR-09, Science Applications International Corporation, Longmont CO, October 2002.

4. Brennan, Terry J. and Troy A. Rhoadarmer. "Performance of a woofer-tweeter deformable mirror control architecture for high-bandwidth high-spatial resolution adaptive optics". *Advanced Wavefront Control: Methods, Devices, and Applications IV*, volume 6306, 63060B–1 – 63060B–12. SPIE, 2006.

5. Brennan, Terry J., Phillip H. Roberts, and David C. Zimmerman. *WaveProp: A Wave Optics Simulation System For Use with MATLAB*. The Optical Sciences Company, Anaheim CA, 2008.

6. Conan, R., C. Bradley, P. Hampton, O. Keskin, A. Hilton, and C. Blain. "Distributed modal command for a two-deformable-mirror adaptive optics system". *Appl. Opt.*, 46(20):4329 – 4340, 2007.

7. Conan, R., P. Hampton, C. Bradley, and O. Keskin. "The woofer-tweeter experiment". *Proceedings of SPIE - The International Society for Optical Engineering*, 6272:62721V –1 – 62721V –10, 2006.

8. Gibson, J.S., C.-C. Chang, and B.L. Ellerbroek. "Adaptive optics: wavefront reconstruction by adaptive filtering and control". *Proceedings of the IEEE Conference on Decision and Control*, 1:761 – 766, 1999.

9. Gibson, J.S., C.-C. Chang, and B.L. Ellerbroek. "Adaptive reconstructors for adaptive optics". *Proceedings of SPIE - The International Society for Optical Engineering*, 3706:326 – 337, 1999.

10. Goodman, Joseph W. *Statistical Optics*. John Wiley and Sons, New York NY, 1985.

11. Hampton, Peter J., Rodolphe Conan, Colin Bradley, and Pan Agathoklis. "Control of a woofer tweeter system of deformable mirrors". *Proceedings of SPIE - The International Society for Optical Engineering*, volume 6274, 62741Z–1 – 62741Z–12. Orlando FL, 2006.

12. Haykin, Simon. *Adaptive Filter Theory*. Prentice Hall, Upper Saddle River NJ, fourth edition, 2002.

13. Honig, Michael L. and David D. Messerschmitt. *Adaptive Filters: Structures, Algorithms, and Applications*. Kluwer Academic Publishers, 1984.

14. Liu, Yu-Tai, N. Chen, and S. Gibson. "Adaptive filtering and control for wavefront reconstruction and jitter control in adaptive optics". *American Control Conference. Proceedings of the 2005*, 2608–2612 vol. 4, June 2005.

15. Liu, Yu-Tai and J. Steve Gibson. "Adaptive control in adaptive optics for directed-energy systems". *Opt. Eng.*, 46(4):046601–1 – 046601–13, 2007.

16. Liu, Yu-Tai and S. Gibson. "Adaptive optics with adaptive filtering and control". *American Control Conference. Proceedings of the 2004*, 4:3176–3179 vol.4, June 2004.

17. Orzechowski, P. K., N. Y. Chen, J. S. Gibson, and T.-C. Tsao. "Optimal Suppression of Laser Beam Jitter by High-Order RLS Adaptive Control". *Control Systems Technology, IEEE Transactions on*, 16(2):255–267, March 2008.

18. Rhoadarmer, Troy A. "Development of a self-referencing interferometer wavefront sensor". *Advanced Wavefront Control: Methods, Devices, and Applications II*, volume 5553, 112–126. SPIE, 2004.

19. Rhoadarmer, Troy A., Laura M. Klein, Steve Gibson, Neil Chen, and Yu-Tai Liu. "Adaptive control and filtering for closed-loop adaptive-optical wavefront reconstruction". Michael K. Giles, John D. Gonglewski, and Richard A. Carreras (editors), *Advanced Wavefront Control: Methods, Devices, and Applications IV*, volume 6306, 63060E. SPIE, 2006.

20. Tyson, Robert K. *Introduction to Adaptive Optics*. SPIE Press, Bellingham WA, 2000.

21. Vitayaudom, Kevin P. *Analysis of Non-Uniform Gain for Control of a Deformable Mirror in an Adaptive-Optics System*. Master's thesis, AFIT/GE/ENG/08-35. School of Engineering and Management, Air Force Institute of Technology (AU), Wright-Patterson AFB OH, March 2008 (ADA482827).

Vita

Captain Jimmie J. Perez earned a Bachelor of Science degree in Electrical Engineering from Brigham Young University in April 2004. He was commissioned in August of 2004 after graduating from Officer Training School, Maxwell AFB, AL. His first assignment was with the Air Force Research Laboratory's Sensors Directorate at Hanscom AFB, MA, as a radar research engineer. In August 2007, he was assigned to the Air Force Institute of Technology, Wright-Patterson AFB, OH, to earn a Master of Science degree in Electrical Engineering. Captain Perez's follow-on assignment is to the 746th Test Squadron at Holloman AFB, NM. Captain Perez is a member of the Eta Kappa Nu Electrical and Computer Engineering Honor Society and the Tau Beta Pi Engineering Honor Society.

REPORT DOCUMENTATION PAGE

Form Approved
OMB No. 0704–0188

1. REPORT DATE *(DD–MM–YYYY)*	2. REPORT TYPE	3. DATES COVERED *(From — To)*
26–03–2009	Master's Thesis	Sept 2007 — Mar 2009

4. TITLE AND SUBTITLE

Adaptive Control Of
Woofer-Tweeter Adaptive Optics

5a. CONTRACT NUMBER

5b. GRANT NUMBER

F2KBAC8308G001

5c. PROGRAM ELEMENT NUMBER

6. AUTHOR(S)

Perez, Jimmie J., Capt, USAF

5d. PROJECT NUMBER

ENG JON 145

5e. TASK NUMBER

5f. WORK UNIT NUMBER

7. PERFORMING ORGANIZATION NAME(S) AND ADDRESS(ES)

Air Force Institute of Technology
Graduate School of Engineering and Management (AFIT/EN)
2950 Hobson Way
WPAFB OH 45433-7765

8. PERFORMING ORGANIZATION REPORT NUMBER

AFIT/GE/ENG/09-33

9. SPONSORING / MONITORING AGENCY NAME(S) AND ADDRESS(ES)

Air Force Research Laboratory
Attn: Dr. Darryl J. Sanchez
3550 Aberdeen Ave SE
Kirtland Air Force Base, NM 87117
(505) 846-7209
darryl.sanchez@kirtland.af.mil

10. SPONSOR/MONITOR'S ACRONYM(S)

AFRL/RDS

11. SPONSOR/MONITOR'S REPORT NUMBER(S)

12. DISTRIBUTION / AVAILABILITY STATEMENT

Approved for public release; distribution is unlimited.

13. SUPPLEMENTARY NOTES

14. ABSTRACT

Adaptive optics applies advanced sensing and control to improve the ability of optical systems to collect images through a turbulent atmosphere. The results of this research effort demonstrate that the combination of two recent approaches improves the performance of adaptive optics in directed energy and laser communication scenarios. The first approach is adaptive control, which offers improved performance over fixed-gain controllers in the presence of rapidly changing turbulence. The second approach incorporated into the study is a dual-mirror system. The two mirrors are a high-bandwidth, low-actuator-stroke (tweeter) mirror and a low-bandwidth, large-actuator-stroke (woofer) mirror. The woofer-tweeter combination allows for better compensation of the large-variance, high-spatial-frequency phase distortion generated by strong turbulence. Two different adaptive controllers are presented. The performance of the different adaptive controllers is compared to each other and to a traditional fixed gain controller. Simulations show that adaptive control of woofer-tweeter AO can increase the mean Strehl ratio by up to 20%.

15. SUBJECT TERMS

adaptive optics, adaptive control systems, control systems, laser communications, directed energy weapons

16. SECURITY CLASSIFICATION OF:			17. LIMITATION OF ABSTRACT	18. NUMBER OF PAGES	19a. NAME OF RESPONSIBLE PERSON
a. REPORT	b. ABSTRACT	c. THIS PAGE			Gregory J. Toussaint, Lt Col, AFIT/ENG
U	U	U	UU	82	19b. TELEPHONE NUMBER *(include area code)* (937) 255–3636, ext 7257; gregory.toussaint@afit.edu